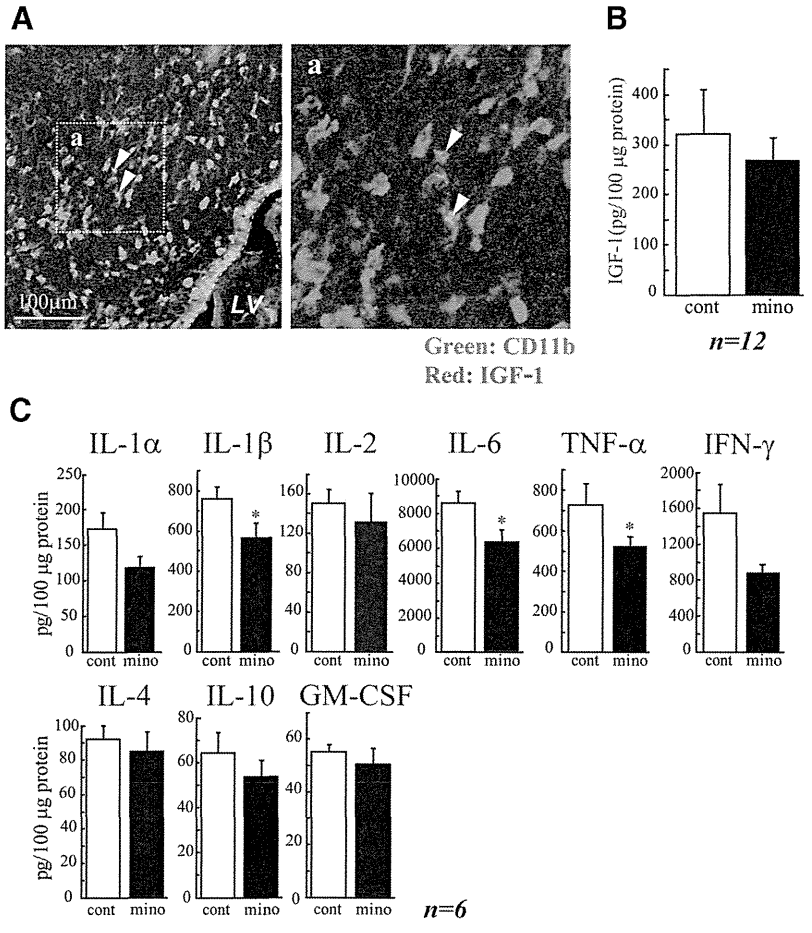

Figure 5. The activated microglia raised the cytokine levels in the SVZ. ***A***, A subpopulation of the microglia express IGF-1 in the early postnatal SVZ, but IGF-1 is not involved in the action of activated microglia during this period. Sagittal sections were immunostained with anti-CD11b (green: microglia) and anti IGF-1 (red) antibodies. Right panel, Magnified image of the square in the left. A subpopulation of microglia is positive for IGF-1 (arrowheads). The percentage of CD11b $^{+}$IGF-1 $^{+}$ was 43.42 ± 6.72% in CD11b $^{+}$ cells. ***B***, Minocycline did not affect the amount of IGF-1 in the early postnatal SVZ. Minocycline was administered by intraperitoneal injection for 3 d beginning at P2 (30 mg/kg/d, P2-P4, n = 6/group), and the amount of IGF-1 in the SVZ was quantified by ELISA. ***C***, Minocycline decreased the amount of inflammatory cytokines in the SVZ. IL-1α, IL-1β, IL-2, IL-4, IL-6, IL-10, GM-CSF, IFN-γ, and TNF-α levels in the SVZ tissue lysate were measured by BioPlex cytokine detection assay system. *$p <$ 0.05 (Student's t test). n = 6 rats/group. Data are mean ± SEM. Similar results were obtained in two independent experiments.

remarkably decreased at P30. These results are consistent with those obtained from the sagittal sections (Fig. 1), showing the population of activated microglia that accumulated within the SVZ during the early postnatal period.

We therefore examined the specific roles of these microglia in the early postnatal SVZ. At early postnatal ages, both neurogenesis and gliogenesis are active in the SVZ (Gould et al., 1999; Wagner et al., 1999; Doetsch and Scharff, 2001; Zerlin et al., 2004; Marshall et al., 2008). To suppress the activation of microglia, we used minocycline, a tetracycline antibiotic, long used to suppress microglial activation (Tikka et al., 2001; Zhao et al., 2007). We first verified the effects of minocycline on the activation of microglia. Minocycline was administered by intraperitoneal injection for 3 d beginning at P2 (30 mg/kg/d, P2-P4, n = 6/group), and sagittal sections of minocycline-treated rat forebrains were immunostained for Iba1, CD11b, and CD68. Minocycline did not change the numbers of Iba1-positive microglia in the VZ/SVZ (Fig. 3*A*, top), but it dramatically changed their shape from amoeboid to more ramified (Fig. 3*A*, bottom). The number of CD11b $^{+}$ cells was significantly decreased (Fig. 3*Bb1*, top and graph), and the decrease in CD11b levels in the SVZ was confirmed by Western blotting (Fig. 3*Bb2*, top graph and photo). The number of CD68 $^{+}$ cells and the level of CD68 were also decreased (Fig. 3*B*, bottom data). These results indicate that our administration of minocycline suppresses the activation of SVZ microglia.

We then investigated the effects of minocycline on early postnatal differentiation. After the administration of minocycline, sagittal sections were immunostained with differentiation markers: Ki67 (proliferating cells), nestin (stem cells), Dcx (neuronal progenitors), PDGFRα (oligodendrocyte progenitors [polydendrocytes]), O1 (oligodendrocyte progenitors [premyelinating oligodendrocytes]), MBP (mature oligodendrocyte [premyelinating and myelinating oligodendrocytes] (Nishiyama et al., 2009), ALDH1L1 (astrocyte progenitors), and S100β $^{+}$ (astrocytes) (Fig. 4*A*). The numbers of cells positive for Ki67, Dcx, O1, and MBP were counted, whereas the levels of nestin, PDGFα, ALDH1L1, and S100β were examined by Western blotting because it was hard to discriminate the cell morphologies by these signals. Minocycline significantly decreased the number of Ki67 $^{+}$ cells and slightly decreased the level of nestin. The number of cells positive for Dcx was also significantly reduced. Furthermore, minocycline decreased the numbers of cells positive for O1 and MBP, whereas the numbers of PDGFRα $^{+}$ cells rather tended to increase. The levels of ALDH1L1 and S100β did not change. These results suggest that activated microglia in the early postnatal SVZ enhance neurogenesis and oligodendrogenesis, and activated microglia affect oligodendrocyte progenitors at rather later stage of differentiation. We also performed the double staining of Ki67 with the respective differentiation markers (Fig. 4*B*). Although the total number of Ki67 $^{+}$ cells was decreased by minocycline, consistent with Figure 4*A*, the percentage of Ki67 $^{+}$ cells also positive for the respective differentiation markers did not change in the absence or presence of minocycline (Fig. 4*B*, left graph), suggesting that minocycline did not affect the proliferation of progenitors of the specific cell types. Typical images of the SVZ cells positive for

←

(*Figure legend continued.*) were examined by Western blotting. Minocycline significantly decreased the number of Ki67 $^{+}$ proliferating cells and decreased the level of nestin. The number of cells positive for Dcx was significantly reduced. Minocycline decreased the numbers of cells positive for O1 and MBP, whereas the expression level of PDGFRα tended to increase. *$p <$ 0.05, **$p <$ 0.01 (Student's t test). n = 6 mice/group. Data are mean ± SEM. ***B***, The ratio of the Ki67 $^{+}$ cells also positive for respective differentiation markers did not change in the absence or presence of minocycline (left graph). Typical images of the cells positive for Ki67 and Nestin, and the cells positive for Ki67 and Dcx in the control group are shown (right panels). We confirmed the same results in three independent experiments.

Ki67 and Nestin, and the cells positive for Ki67 and Dcx in the control group are shown (Fig. 4*B*, right panels).

Butovsky et al. (2006a) have reported that IGF-1 released from activated microglia promoted neurogenesis and oligodendrogenesis from adult stem/progenitor cells. We examined whether microglia in the early postnatal SVZ produce IGF-1 (Fig. 5*A*). Microglia did contain IGF-1 protein, but the percentage of $CD11b^+$ cells also positive for $IGF\text{-}1^+$ was 43.42 ± 6.72%. Furthermore, the amount of IGF-1 in the SVZ tissue lysates was not decreased by minocycline (Fig. 5*B*). These results suggest that, although a fraction of activated microglia in the early postnatal SVZ did produce IGF-1, the effects of activated microglia on neurogenesis and oligodendrogenesis obtained in our study were independent of IGF-1. Activated microglia release a number of cytokines. In some cases other than pathological conditions, cytokines also have physiological roles (Schäfers and Sorkin, 2008; Spedding and Gressens, 2008; Camacho-Arroyo et al., 2009; Miller et al., 2009; Spooren et al., 2011). We therefore investigated whether the SVZ microglia cause the increase in cytokine concentrations in the early postnatal SVZ (Fig. 5*C*). We examined the effects of minocycline on the levels of IL-1α, IL-1β, IL-2, IL-4, IL-6, IL-10, GM-CSF, IFN-γ, and TNF-α. To measure multiple cytokines in a small volume of tissue samples simultaneously, we used the BioPlex cytokine detection assay system (Bio-Rad). The levels of IL-1β, IL-6, and TNF-α were significantly decreased by the 3-day intraperitoneal administration of minocycline (Fig. 5*C*). Although the difference was not significant, the level of IFN-γ also tended to be decreased.

To examine more directly whether these cytokines affected neurogenesis and oligodendrogenesis, we performed *in vitro* experiments, coculturing neural stem cells with activated microglia. Microglia cultured independently of neurospheres on transwells were activated by LPS (10 ng/ml, 30 min) in the presence or absence of minocycline (10 μM). The microglia were carefully washed to remove residual LPS and minocycline, and then the transwell on which microglia were cultured was set onto the neurosphere cultures in prodifferentiation conditions. The activated microglia significantly increased the number of $\beta3\text{-tubulin}^+$ and $O4^+$ cells but had no effects on $GFAP^+$ cells in neurospheres (Fig. 6*A*,*B*). Minocycline almost completely suppressed the effects of activated microglia on the numbers of cells positive

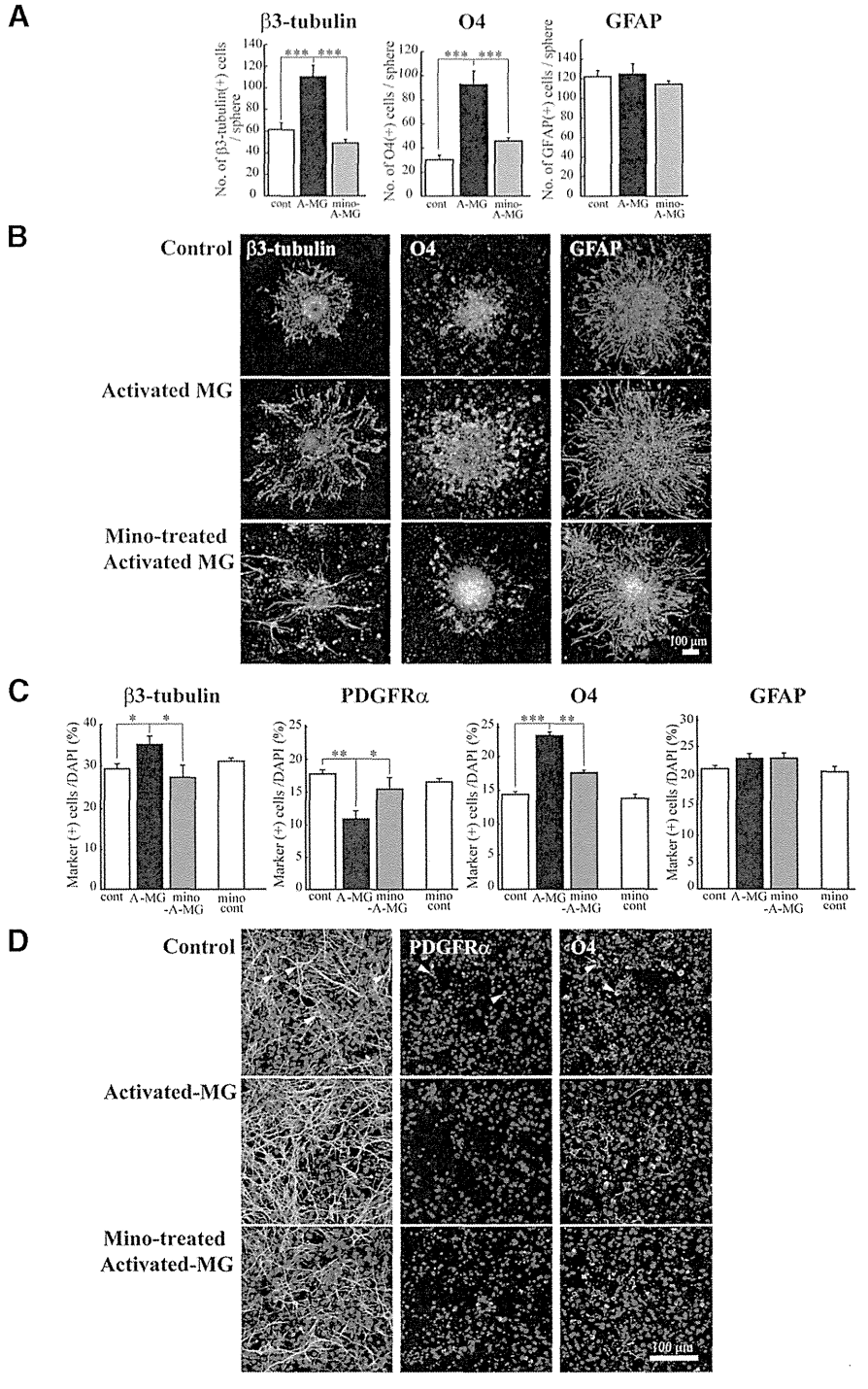

Figure 6. The reproduction of the enhancement of neurogenesis and oligodendrogenesis by activated microglia *in vitro*. Microglia cultured independently of neurosphere on transwells were activated by LPS (10 ng/ml, 30 min) in the presence or absence of minocycline (10 μM), washed carefully, and the transwells were set onto the neurospheres or dissociated cells from neurosphere in prodifferentiation conditions. After differentiation periods suitable for neurons (7 d) or oligodendrocytes (11 d), neurospheres were stained for β3-tubulin (green), PDGFRα (green), O4 (green), GFAP (red), and TOTO3 (cyan). To check the effects of minocycline alone, dissociated cells were incubated in the presence of minocycline (10 μM) for 7 d. ***A***, Quantification of the numbers of neurons, oligodendrocyte progenitors, or astrocytes differentiated from neurospheres cocultured with activated microglia in the presence or absence of minocycline. $^{***}p < 0.001$ (Tukey's test by ANOVA). $n = 12$ neurospheres/group. Data are mean ± SEM. ***B***, Representative immunostained images of neurospheres cocultured with activated microglia in the presence or absence of minocycline. ***C***, The effects of activated microglia on differentiation of single cells dissociated from neurospheres in the presence or absence of minocycline. The effects of minocycline alone were also shown (mino-cont in each graph). $^{*}p < 0.05$, $^{**}p < 0.01$, $^{***}p < 0.001$. (Tukey's test by ANOVA). $n = 12$ neurospheres/group. Data are mean ± SEM. ***D***, Images of cells immunostained for differentiation markers. Arrowheads indicate the representative cells positive for the differentiation markers.

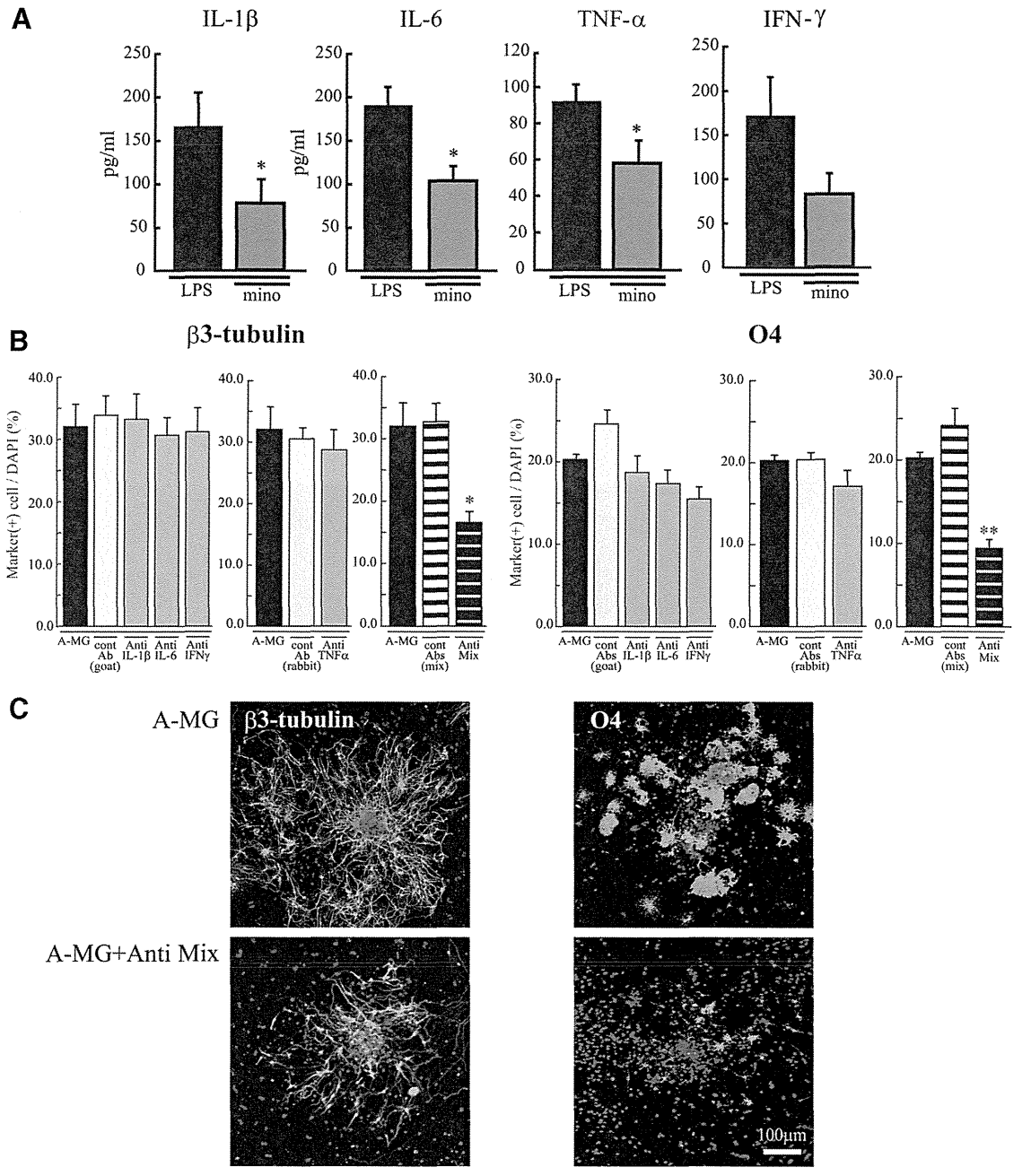

Figure 7. The *in vitro* enhancement of neurogenesis and oligodendrogenesis by activated microglia was suppressed by the mixture of function-blocking antibodies (anti-IL-1β, anti-IL-6, anti-TNF-α, and anti-IFN-γ). ***A***, The release of IL-1β, IL-6, TNF-α, or IFN-γ from activated microglia was suppressed by minocycline. Cultured microglia were activated by LPS (10 ng/ml, 30 min) in the absence and presence of minocycline (10 μM). The concentration of each cytokine in the supernatant was measured by ELISA 24 h after. *$p < 0.05$ (Student's *t* test). Data are mean ± SEM. ***B***, Effects of function-blocking antibodies to IL-1β, IL-6, TNF-α, and IFN-γ on enhanced neurogenesis and oligodendrogenesis by the activated microglia. The neurospheres were differentiated in the absence or presence of functional blocking antibodies (goat anti-rat IL-1β antibody, goat anti-rat IL-6 antibody, TNF-α antibody, or goat anti-mouse/rat IFN-γ antibody) (1 μg/ml for each) and a mixture of all of these antibodies. After a differentiation period suitable for neurons (7 d) or oligodendrocytes (11 d), neurospheres were stained for β3-tubulin (green), O4 (green), and TOTO3 (cyan). The data of single function blocking antibodies were compared with the controls, which include the same concentration of isotype-matched control IgGs (1 μg/ml for each). The data of the mixture of function blocking antibodies were compared with the controls, which include the same concentrations of isotype-matched control IgGs (i.e., 3 μg/ml of normal goat IgG control and 1 μg/ml of rabbit IgG control). *$p < 0.05$. **$p < 0.01$, versus isotype-matched control IgG group (Tukey's test by ANOVA). Data are mean ± SEM. ***C***, Representative immunostained images of neurospheres cocultured with activated microglia in the absence or presence of the mixture of the function-blocking antibodies. We confirmed the same results in three independent experiments.

for β3-tubulin or O4. We further confirmed these results using a differentiation assay with cells dissociated from neurospheres (Fig. 6*C*,*D*). With this protocol, the morphology of each cell could be discriminated more clearly. Consistent with the results described above, an increase in the numbers of cells positive for β3-tubulin and O4 was induced by activated microglia (Fig. 6*C*,*D*). Of note, PDGFRα^+ cells were decreased by activated microglia, whereas O4$^+$ cells were increased by activated microglia. Minocycline suppressed both of these effects, suggesting that activated microglia affect the later stage of oligodendrogenesis, thereby reducing the size of PDGFα^+ progenitor pool. In this experiment, we also checked the effects of minocycline alone (10 μM) on neurogenesis and oligodendrogenesis (Fig. 6*C*, "mino-cont" in each graph). Minocycline did not affect the numbers of

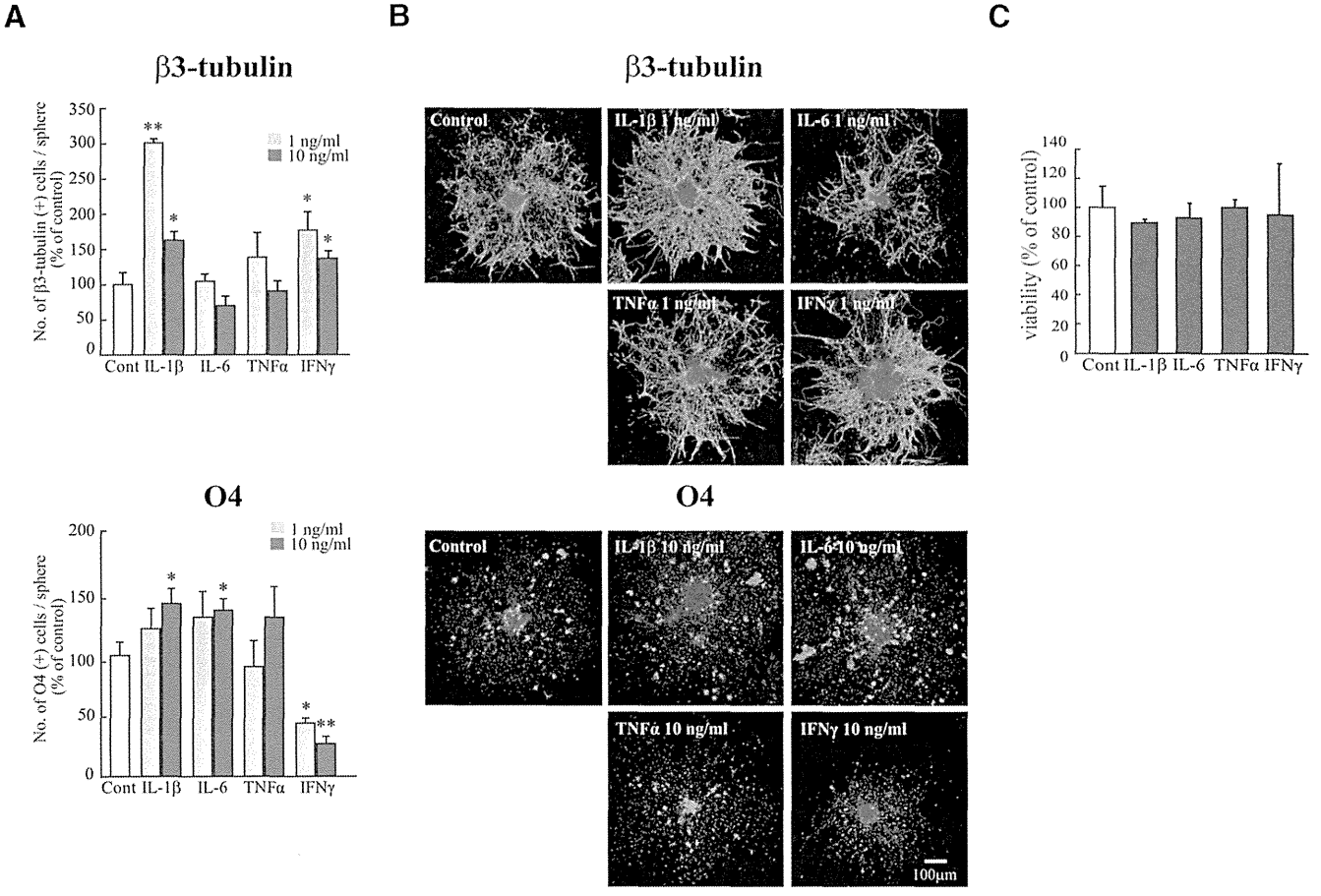

Figure 8. The effect of each cytokine on neurogenesis and oligodendrogenesis. Neurospheres were incubated for differentiation period suitable for neurons (7 d) or oligodendrocytes (11 d) in the presence of each single cytokine (rIL-1β, rIL-6, rTNF-α, or rIFN-γ) at 1–10 ng/ml. Neurospheres were stained for β3-tubulin (green), O4 (green), followed by TOTO3 (cyan). ***A***, Quantification of the effects of cytokines on neurogenesis and oligodendrogenesis. IL-1β and IFN-γ significantly enhanced neurogenesis at 1 ng/ml. IL-1β and IL-6 enhanced oligodendrogenesis at 10 ng/ml. $^*p < 0.05$ versus control (Tukey's test by ANOVA). $^{**}p < 0.01$ versus control (Tukey's test by ANOVA). $n = 8$ neurospheres/group. Data are mean ± SEM. ***B***, Representative images of neurospheres immunostained for β3-tubulin and O4 after differentiation in the presence of the cytokine. ***C***, The effect of each cytokine (10 ng/ml) on cell viability. They did not affect cell viability at 10 ng/ml. The same results were obtained in two independent experiments.

cells positive for β3-tubulin, O4, PDGFRα, or GFAP, indicating that minocycline itself had little direct effects on neurogenesis and oligodendrogenesis. Together, these results demonstrated that we could reproduce the *in vivo* data in an *in vitro* coculture experiment. We further confirmed that activated microglia enhanced neurogenesis and oligodendrogenesis, and minocycline specifically suppressed the effects of microglia. We therefore examined the effects of minocycline on the release of IL-1β, IL-6, TNF-α, and IFN-γ from activated microglia *in vitro*. In the presence of minocycline, the release of all of these cytokines was significantly suppressed (Fig. 7*A*), consistent with *in vivo* data (Fig. 5*C*). To examine the extent of the contribution of each cytokine to the enhancement of neurogenesis and oligodendrogenesis, we applied function-blocking antibodies to IL-1β, IL-6, TNF-α, and IFN-γ (1 μg/ml) to cocultures of activated microglia and neurospheres (Fig. 7*B*). The same concentration of isotype-matched control IgG (both of goat and rabbit) (1 μg/ml) did not have any effects on either neurogenesis or oligodendrogenesis. Unexpectedly, any single function-blocking antibody to IL-1β, IL-6, TNF-α, or IFN-γ did not change the effects of activated microglia on neurogenesis and oligodendrogenesis (Fig. 7*B*). We then tried a mixture of all of these function-blocking antibodies (goat anti-rat IL-1β antibody, goat anti-rat IL-6 antibody, TNF-α antibody, and goat anti-mouse/rat IFN-γ antibody, 1 μg/ml for each). When compared with the control which included the same concentrations of isotype-matched control IgGs (i.e., 3 μg/ml of normal goat IgG control and 1 μg/ml of rabbit IgG control), the effects of activated microglia were significantly suppressed by a mixture of all of these function-blocking antibodies (Fig. 7*B*, Anti Mix in the right graphs in β3-tubulin and O4, respectively). The representative images of the expression of β3-tubulin (left) or O4 (right) in neurospheres cocultured with activated microglia in the presence of the mixture of function-blocking antibodies are shown in Figure 7*C*. We also examined the direct effects of each single cytokine on neurogenesis and oligodendrogenesis separately (Fig. 8). IL-1β and IFN-γ enhanced neurogenesis at 1 ng/ml, although the effects became weaker at 10 ng/ml (Fig. 8*A*). IL-1β and IL-6 enhanced oligodendrogenesis at 10 ng/ml (Fig. 8*A*). IFN-γ suppressed oligodendrogenesis. These results suggest that IL-1β and IFN-γ are important for neurogenesis, whereas IL-1β and IL-6 are important for oligodendrogenesis, and the combinations and concentrations optimal for neurogenesis and oligodendrogenesis are different. Representative data of the neurospheres treated with the cytokines are shown in Figure 8*B*. We confirmed that each single cytokine did not affect cell viability at 10 ng/ml in our experimental protocol (Fig. 8*C*). These *in vitro* data indicate that activated microglia regulate neurogenesis and oligodendrogenesis through released cytokines, and the cyto-

kines produce their effects in a synergistic manner. It also appears that the combinations and concentrations optimal for neurogenesis and oligodendrogenesis are different.

Discussion

In the postnatal mammalian brain, neural stem cells (NSCs) are mainly localized in two areas: the forebrain SVZ (Doetsch and Scharff, 2001) and the subgranular zone of the dentate gyrus (Zerlin et al., 2004) of the hippocampus (Gould et al., 1999; Lie et al., 2004). The microenvironments that are permissive for neurogenesis and gliogenesis are composed of a variety of cell types, such as stem cells, progenitor cells, astrocyte cells, and microglial cells. Increasing evidence indicates the importance of the surrounding glial cells in neurogenesis (Doetsch et al., 1999; Temple, 2001). Goings et al. (2006) have shown that microglia in the adult SVZ are semiactivated, but microglial contribution to neurogenesis is complex. So far, the role of microglia in neurogenesis has been examined mainly in pathological conditions (Ekdahl et al., 2003; Monje et al., 2003). Activated microglia in inflammatory settings, such as intraperitoneal administration of LPS, inhibited neurogenesis (Ekdahl et al., 2003; Monje et al., 2003; Cacci et al., 2008). However, a growing number of studies have suggested that activated microglia are beneficial for neurogenesis (Aarum et al., 2003; Butovsky et al., 2005, 2006a; Walton et al., 2006; Ziv et al., 2006; Hanisch and Kettenmann, 2007; Ekdahl et al., 2009; Bachstetter et al., 2011; Ekdahl, 2012; Vukovic et al., 2012), even in pathological conditions, such as an animal model of multiple sclerosis (Butovsky et al., 2006b), ischemia (Thored et al., 2009; Deierborg et al., 2010), and epilepsy (Bonde et al., 2006). Such variability concerning the effects of microglia on neurogenesis may reflect the different polarization of microglia and/or the precise status of NSCs/neuronal progenitor cells (NPCs) (Cacci et al., 2008; Li et al., 2010; Ekdahl, 2012; Ortega et al., 2013), and crosstalk between them (Mosher et al., 2012).

Concerning the origin of microglia, various data have been reported. *In vivo* lineage tracing studies have established that microglia differentiate from primitive myeloid progenitors that arise before embryonic day 8 and are identified in the CNS parenchyma even before definitive hematopoiesis (Ginhoux et al., 2010), although it has been shown that microglia migrate from lateral ventricle into brain via SVZ in the postnatal brain (Mohri et al., 2003). Microglia in the embryonic SVZ limit the production of cortical neurons by phagocytosing neural precursor cells (Cunningham et al., 2013). Even in the adult brain, microglia appear densely populated in neurogenic niches, such as the SVZ (Mosher et al., 2012), and appear more activated in the adult SVZ than in non-neurogenic zones (Goings et al., 2006). Although these data strongly suggest that microglia play important roles in CNS development and an increasing number of studies have elucidated various roles of microglia during developmental periods (Wu et al., 1993; Pont-Lezica et al., 2011; Tremblay et al., 2011), the detailed dynamics of microglia in the SVZ from early postnatal stages to a young adult stage remain to be elucidated. Furthermore, few studies have examined the role of microglia in normal developmental processes during this period. In this study, we found that activated microglia first accumulated in the SVZ and then dispersed to white matter, where they became more ramified. In addition, the number of activated microglia was largest in the medial SVZ throughout the studied period (P30). We here elucidated that activated microglia in the early postnatal SVZ enhance neurogenesis and oligodendrogenesis through the mechanisms described below. Our present data and the previous reports concerning developmental changes in the distribution suggest that the developmental roles of microglia in the SVZ are not transient but more general throughout life.

Using a combination of *in vivo* and *in vitro* approaches, we demonstrated that these activated microglia in the early postnatal SVZ enhanced neurogenesis and oligodendrogenesis through releasing cytokines. Butovsky et al. (2006a) reported that the beneficial effects of microglia on adult neurogenesis/oligodendrogenesis was achieved by IGF-1 after IL-4 and IFN-γ release from activated microglia. In our study, although the activated microglia in the early postnatal SVZ did produce IGF-1, the effects of activated microglia on neurogenesis and oligodendrogenesis observed here were independent of IGF-1. We clarified that the SVZ microglia facilitate neurogenesis and oligodendrogenesis via production of cytokines. Interestingly, in *in vitro* coculture experiments, the enhancement of neurogenesis and oligodendrogenesis was suppressed by a mixture of function-blocking antibodies (anti-IL-1β, anti-IL-6, anti-TNF-α, anti-IFN-γ), but not by a single function-blocking antibody. These results suggest that microglial cytokines enhance neurogenesis and oligodendrogenesis in combinations. In support of this, among the cytokines we examined, only IL-1β and IFN-γ enhanced neurogenesis, whereas only IL-1β and IL-6 showed potentials of enhancing oligodendrogenesis. Previous reports have shown that NPCs express IL-1β, IL-1RI and IL-1RII, and IL-1β regulates the proliferation and differentiation of NPCs (Wang et al., 2007). It has been shown that IL-1β promotes proliferation and differentiation of oligodendrocyte progenitor cells (Vela et al., 2002). Furthermore, IL-6 and IL-6R are reported to promote neurogenesis and gliogenesis (Islam et al., 2009; Oh et al., 2010). Li et al. (2010) showed that IFN-γ stimulated neurosphere formation from embryonic brain, but the effects of IFN-γ are modified in the presence of microglia, supporting the complementary interactions between cytokines.

These proinflammatory cytokines had been thought to cause suppression of neurogenesis in pathological conditions, such as chronic LPS stimulation (Monje et al., 2003), allergic encephalomyelitis (Ben-Hur et al., 2003), and status epilepticus (Iosif et al., 2006; Koo and Duman, 2008). However, recent reports have shown that that the different polarizations of microglia are induced by different application protocols of LPS (Cacci et al., 2008), suggesting that the combination and the concentration of cytokines released by microglia change depending on the ambient conditions. Indeed, some previous reports suggest that each cytokine reveals different effects at different concentrations (Bernardino et al., 2008; Cacci et al., 2008; Das and Basu, 2008; Russo et al., 2011). Bernardino et al. (2008) have shown that TNF-α results in proliferation of neural stem cells at 1 ng/ml but caused apoptosis at 10–100 ng/ml. Microglia in the developmental brains may sense the change of environment and release a certain combination of cytokines at suitable concentrations for neurogenesis and oligodendrogenesis, whereas overactivation of microglia in pathological inflammation or nerve injury induces massive proinflammatory cytokine production, resulting in the suppression of neurogenesis. Nakanishi et al. (2007) showed that IL-6 promoted astrocytogenesis from the SVZ neurospheres. In our study, however, although activated microglia release IL-6, the effects on astrocytogenesis were not observed either *in vivo* or *in vitro*. This might be because of different medium compositions (i.e., growth factors) used for differentiation of neurosphere. Compared with the other cytokines, only IFN-γ suppressed oligodendrogenesis, suggesting that a proper concentration range of IFN-γ to enhance oligodendrogenesis might be narrower than the other cytokines.

Of interest, our results suggest that activated microglia significantly increased $O4^+$ cells while decreasing $PDGFR\alpha^+$ cells. These results suggest that activated microglia enhance oligodendrogenesis at later stages of oligodendrocyte differentiation. Recently, Miron et al. (2013) showed that a switch from M1 to M2 occurred in microglia during remyelination, and oligodendrocyte differentiation was enhanced by M2 cell releasing factors. A comprehensive analysis about the released factors from microglia, including cytokines, and the precise identification of the cell population (NSCs and/or NPCs) that are responsive to these factors will be necessary to understand fully the mechanisms underlying the effects of microglia on neurogenesis and gliogenesis.

In conclusion, we have found a population of activated microglia accumulating in the early postnatal SVZ that facilitate neurogenesis and oligodendrogenesis. A synergism among cytokines was important for the effects. To our knowledge, this is the first report to show that microglia regulate cell differentiation via releasing cytokines in early postnatal brain development.

References

Aarum J, Sandberg K, Haeberlein SL, Persson MA (2003) Migration and differentiation of neural precursor cells can be directed by microglia. Proc Natl Acad Sci U S A 100:15983–15988. CrossRef Medline

Bachstetter AD, Morganti JM, Jernberg J, Schlunk A, Mitchell SH, Brewster KW, Hudson CE, Cole MJ, Harrison JK, Bickford PC, Gemma C (2011) Fractalkine and CX 3 CR1 regulate hippocampal neurogenesis in adult and aged rats. Neurobiol Aging 32:2030–2044. CrossRef Medline

Ben-Hur T, Ben-Menachem O, Furer V, Einstein O, Mizrachi-Kol R, Grigoriadis N (2003) Effects of proinflammatory cytokines on the growth, fate, and motility of multipotential neural precursor cells. Mol Cell Neurosci 24:623–631. CrossRef Medline

Bernardino L, Agasse F, Silva B, Ferreira R, Grade S, Malva JO (2008) Tumor necrosis factor-alpha modulates survival, proliferation, and neuronal differentiation in neonatal subventricular zone cell cultures. Stem Cells 26:2361–2371. CrossRef Medline

Bonde S, Ekdahl CT, Lindvall O (2006) Long-term neuronal replacement in adult rat hippocampus after status epilepticus despite chronic inflammation. Eur J Neurosci 23:965–974. CrossRef Medline

Butovsky O, Talpalar AE, Ben-Yaakov K, Schwartz M (2005) Activation of microglia by aggregated beta-amyloid or lipopolysaccharide impairs MHC-II expression and renders them cytotoxic whereas IFN-gamma and IL-4 render them protective. Mol Cell Neurosci 29:381–393. CrossRef Medline

Butovsky O, Ziv Y, Schwartz A, Landa G, Talpalar AE, Pluchino S, Martino G, Schwartz M (2006a) Microglia activated by IL-4 or IFN-gamma differentially induce neurogenesis and oligodendrogenesis from adult stem/progenitor cells. Mol Cell Neurosci 31:149–160. CrossRef Medline

Butovsky O, Landa G, Kunis G, Ziv Y, Avidan H, Greenberg N, Schwartz A, Smirnov I, Pollack A, Jung S, Schwartz M (2006b) Induction and blockage of oligodendrogenesis by differently activated microglia in an animal model of multiple sclerosis. J Clin Invest 116:905–915. CrossRef Medline

Cacci E, Ajmone-Cat MA, Anelli T, Biagioni S, Minghetti L (2008) In vitro neuronal and glial differentiation from embryonic or adult neural precursor cells are differently affected by chronic or acute activation of microglia. Glia 56:412–425. CrossRef Medline

Camacho-Arroyo I, López-Griego L, Morales-Montor J (2009) The role of cytokines in the regulation of neurotransmission. Neuroimmunomodulation 16:1–12. CrossRef Medline

Cunningham CL, Martínez-Cerdeño V, Noctor SC (2013) Microglia regulate the number of neural precursor cells in the developing cerebral cortex. J Neurosci 33:4216–4233. CrossRef Medline

Das S, Basu A (2008) Inflammation: a new candidate in modulating adult neurogenesis. J Neurosci Res 86:1199–1208. CrossRef Medline

Deierborg T, Roybon L, Inacio AR, Pesic J, Brundin P (2010) Brain injury activates microglia that induce neural stem cell proliferation ex vivo and promote differentiation of neurosphere-derived cells into neurons and oligodendrocytes. Neuroscience 171:1386–1396. CrossRef Medline

Doetsch F, Scharff C (2001) Challenges for brain repair: insights from adult neurogenesis in birds and mammals. Brain Behav Evol 58:306–322. CrossRef Medline

Doetsch F, García-Verdugo JM, Alvarez-Buylla A (1999) Regeneration of a germinal layer in the adult mammalian brain. Proc Natl Acad Sci U S A 96:11619–11624. CrossRef Medline

Ekdahl CT (2012) Microglial activation- tuning and pruning adult neurogenesis. Front Pharmacol 3:41. CrossRef Medline

Ekdahl CT, Claasen JH, Bonde S, Kokaia Z, Lindvall O (2003) Inflammation is detrimental for neurogenesis in adult brain. Proc Natl Acad Sci U S A 100:13632–13637. CrossRef Medline

Ekdahl CT, Kokaia Z, Lindvall O (2009) Brain inflammation and adult neurogenesis: the dual role of microglia. Neuroscience 158:1021–1029. CrossRef Medline

Ginhoux F, Greter M, Leboeuf M, Nandi S, See P, Gokhan S, Mehler MF, Conway SJ, Ng LG, Stanley ER, Samokhvalov IM, Merad M (2010) Fate mapping analysis reveals that adult microglia derive from primitive macrophages. Science 330:841–845. CrossRef Medline

Goings GE, Kozlowski DA, Szele FG (2006) Differential activation of microglia in neurogenic versus non-neurogenic regions of the forebrain. Glia 54:329–342. CrossRef Medline

Gould E, Reeves AJ, Graziano MS, Gross CG (1999) Neurogenesis in the neocortex of adult primates. Science 286:548–552. CrossRef Medline

Hamanoue M, Matsuzaki Y, Sato K, Okano HJ, Shibata S, Sato I, Suzuki S, Ogawara M, Takamatsu K, Okano H (2009) Cell surface N-glycans mediated isolation of mouse neural stem cells. J Neurochem 110:1575–1584. CrossRef Medline

Hanisch UK, Kettenmann H (2007) Microglia: active sensor and versatile effector cells in the normal and pathologic brain. Nat Neurosci 10:1387–1394. CrossRef Medline

Hirasawa T, Ohsawa K, Imai Y, Ondo Y, Akazawa C, Uchino S, Kohsaka S (2005) Visualization of microglia in living tissues using Iba1-EGFP transgenic mice. J Neurosci Res 81:357–362. CrossRef Medline

Ignácio AR, Müller YM, Carvalho MS, Nazari EM (2005) Distribution of microglial cells in the cerebral hemispheres of embryonic and neonatal chicks. Braz J Med Biol Res 38:1615–1621. Medline

Inoue K (2008) Purinergic systems in microglia. Cell Mol Life Sci 65:3074–3080. CrossRef Medline

Iosif RE, Ekdahl CT, Ahlenius H, Pronk CJ, Bonde S, Kokaia Z, Jacobsen SE, Lindvall O (2006) Tumor necrosis factor receptor 1 is a negative regulator of progenitor proliferation in adult hippocampal neurogenesis. J Neurosci 26:9703–9712. CrossRef Medline

Islam O, Gong X, Rose-John S, Heese K (2009) Interleukin-6 and neural stem cells: more than gliogenesis. Mol Biol Cell 20:188–199. CrossRef Medline

Kettenmann H, Hanisch UK, Noda M, Verkhratsky A (2011) Physiology of microglia. Physiol Rev 91:461–553. CrossRef Medline

Koo JW, Duman RS (2008) IL-1beta is an essential mediator of the antineurogenic and anhedonic effects of stress. Proc Natl Acad Sci U S A 105:751–756. CrossRef Medline

Li L, Walker TL, Zhang Y, Mackay EW, Bartlett PF (2010) Endogenous interferon gamma directly regulates neural precursors in the non-inflammatory brain. J Neurosci 30:9038–9050. CrossRef Medline

Lie DC, Song H, Colamarino SA, Ming GL, Gage FH (2004) Neurogenesis in the adult brain: new strategies for central nervous system diseases. Annu Rev Pharmacol Toxicol 44:399–421. CrossRef Medline

Marshall GP 2nd, Demir M, Steindler DA, Laywell ED (2008) Subventricular zone microglia possess a unique capacity for massive in vitro expansion. Glia 56:1799–1808. CrossRef Medline

Miller RJ, Jung H, Bhangoo SK, White FA (2009) Cytokine and chemokine regulation of sensory neuron function. Handb Exp Pharmacol 194:417–449. CrossRef Medline

Miron VE, Boyd A, Zhao JW, Yuen TJ, Ruckh JM, Shadrach JL, van Wijngaarden P, Wagers AJ, Williams A, Franklin RJ, ffrench-Constant C (2013) M2 microglia and macrophages drive oligodendrocyte differentiation during CNS remyelination. Nat Neurosci 16:1211–1218. CrossRef Medline

Mohri I, Eguchi N, Suzuki K, Urade Y, Taniike M (2003) Hematopoietic prostaglandin D synthase is expressed in microglia in the developing postnatal mouse brain. Glia 42:263–274. CrossRef Medline

Monje ML, Toda H, Palmer TD (2003) Inflammatory blockade restores adult hippocampal neurogenesis. Science 302:1760–1765. CrossRef Medline

Monji A, Kato T, Kanba S (2009) Cytokines and schizophrenia: microglia

hypothesis of schizophrenia. Psychiatry Clin Neurosci 63:257–265. CrossRef Medline

Mosher KI, Andres RH, Fukuhara T, Bieri G, Hasegawa-Moriyama M, He Y, Guzman R, Wyss-Coray T (2012) Neural progenitor cells regulate microglia functions and activity. Nat Neurosci 15:1485–1487. CrossRef Medline

Nakajima K, Kohsaka S (2001) Microglia: activation and their significance in the central nervous system. J Biochem 130:169–175. CrossRef Medline

Nakajima K, Tsuzaki N, Shimojo M, Hamanoue M, Kohsaka S (1992) Microglia isolated from rat brain secrete a urokinase-type plasminogen activator. Brain Res 577:285–292. CrossRef Medline

Nakanishi M, Niidome T, Matsuda S, Akaike A, Kihara T, Sugimoto H (2007) Microglia-derived interleukin-6 and leukaemia inhibitory factor promote astrocytic differentiation of neural stem/progenitor cells. Eur J Neurosci 25:649–658. CrossRef Medline

Nishiyama A, Komitova M, Suzuki R, Zhu X (2009) Polydendrocytes (NG2 cells): multifunctional cells with lineage plasticity. Nat Rev Neurosci 10: 9–22. CrossRef Medline

Oh J, McCloskey MA, Blong CC, Bendickson L, Nilsen-Hamilton M, Sakaguchi DS (2010) Astrocyte-derived interleukin-6 promotes specific neuronal differentiation of neural progenitor cells from adult hippocampus. J Neurosci Res 88:2798–2809. CrossRef Medline

Ortega F, Gascón S, Masserdotti G, Deshpande A, Simon C, Fischer J, Dimou L, Chichung Lie D, Schroeder T, Berninger B (2013) Oligodendrogliogenic and neurogenic adult subependymal zone neural stem cells constitute distinct lineages and exhibit differential responsiveness to Wnt signalling. Nat Cell Biol 15:602–613. CrossRef Medline

Pont-Lezica L, Béchade C, Belarif-Cantaut Y, Pascual O, Bessis A (2011) Physiological roles of microglia during development. J Neurochem 119: 901–908. CrossRef Medline

Reynolds BA, Tetzlaff W, Weiss S (1992) A multipotent EGF-responsive striatal embryonic progenitor cell produces neurons and astrocytes. J Neurosci 12:4565–4574. Medline

Russo I, Barlati S, Bosetti F (2011) Effects of neuroinflammation on the regenerative capacity of brain stem cells. J Neurochem 116:947–956. CrossRef Medline

Schäfers M, Sorkin L (2008) Effect of cytokines on neuronal excitability. Neurosci Lett 437:188–193. CrossRef Medline

Spedding M, Gressens P (2008) Neurotrophins and cytokines in neuronal plasticity. Novartis Found Symp 289:222–233; discussion 233–240. Medline

Spooren A, Kolmus K, Laureys G, Clinckers R, De Keyser J, Haegeman G, Gerlo S (2011) Interleukin-6, a mental cytokine. Brain Res Rev 67:157–183. CrossRef Medline

Suzuki SO, Goldman JE (2003) Multiple cell populations in the early postnatal subventricular zone take distinct migratory pathways: a dynamic study of glial and neuronal progenitor migration. J Neurosci 23:4240–4250. Medline

Temple S (2001) The development of neural stem cells. Nature 414:112–117. CrossRef Medline

Thored P, Heldmann U, Gomes-Leal W, Gisler R, Darsalia V, Taneera J, Nygren JM, Jacobsen SE, Ekdahl CT, Kokaia Z, Lindvall O (2009) Long-term accumulation of microglia with proneurogenic phenotype concomitant with persistent neurogenesis in adult subventricular zone after stroke. Glia 57:835–849. CrossRef Medline

Tikka T, Fiebich BL, Goldsteins G, Keinanen R, Koistinaho J (2001) Minocycline, a tetracycline derivative, is neuroprotective against excitotoxicity by inhibiting activation and proliferation of microglia. J Neurosci 21: 2580–2588. Medline

Tremblay MÈ, Stevens B, Sierra A, Wake H, Bessis A, Nimmerjahn A (2011) The role of microglia in the healthy brain. J Neurosci 31:16064–16069. CrossRef Medline

Vela JM, Molina-Holgado E, Arévalo-Martín A, Almazán G, Guaza C (2002) Interleukin-1 regulates proliferation and differentiation of oligodendrocyte progenitor cells. Mol Cell Neurosci 20:489–502. CrossRef Medline

Vukovic J, Colditz MJ, Blackmore DG, Ruitenberg MJ, Bartlett PF (2012) Microglia modulate hippocampal neural precursor activity in response to exercise and aging. J Neurosci 32:6435–6443. CrossRef Medline

Wagner JP, Black IB, DiCicco-Bloom E (1999) Stimulation of neonatal and adult brain neurogenesis by subcutaneous injection of basic fibroblast growth factor. J Neurosci 19:6006–6016. Medline

Walton NM, Sutter BM, Laywell ED, Levkoff LH, Kearns SM, Marshall GP 2nd, Scheffler B, Steindler DA (2006) Microglia instruct subventricular zone neurogenesis. Glia 54:815–825. CrossRef Medline

Wang X, Fu S, Wang Y, Yu P, Hu J, Gu W, Xu XM, Lu P (2007) Interleukin-1beta mediates proliferation and differentiation of multipotent neural precursor cells through the activation of SAPK/JNK pathway. Mol Cell Neurosci 36:343–354. CrossRef Medline

Wu CH, Wen CY, Shieh JY, Ling EA (1993) A quantitative study of the differentiation of microglial cells in the developing cerebral cortex in rats. J Anat 182:403–413. Medline

Xu J, Ling EA (1994) Studies of the distribution and functional roles of transitory amoeboid microglial cells in developing rat brain using exogenous horseradish peroxidase as a marker. J Hirnforsch 35:103–111. Medline

Zerlin M, Milosevic A, Goldman JE (2004) Glial progenitors of the neonatal subventricular zone differentiate asynchronously, leading to spatial dispersion of glial clones and to the persistence of immature glia in the adult mammalian CNS. Dev Biol 270:200–213. CrossRef Medline

Zhao C, Ling Z, Newman MB, Bhatia A, Carvey PM (2007) TNF-alpha knockout and minocycline treatment attenuates blood–brain barrier leakage in MPTP-treated mice. Neurobiol Dis 26:36–46. CrossRef Medline

Ziv Y, Ron N, Butovsky O, Landa G, Sudai E, Greenberg N, Cohen H, Kipnis J, Schwartz M (2006) Immune cells contribute to the maintenance of neurogenesis and spatial learning abilities in adulthood. Nat Neurosci 9:268–275. CrossRef Medline

Bioconjugate Chemistry

Communication

pubs.acs.org/bc

Development of Cell-Penetrating R7 Fragment-Conjugated Helical Peptides as Inhibitors of Estrogen Receptor-Mediated Transcription

Takaya Nagakubo,[†,‡] Yosuke Demizu,[*,†] Yasunari Kanda,[†] Takashi Misawa,[†] Takuji Shoda,[†] Keiichiro Okuhira,[†] Yuko Sekino,[†] Mikihiko Naito,[†] and Masaaki Kurihara[*,†,‡]

[†]National Institute of Health Sciences, Tokyo 158-8501, Japan

[‡]Graduate School of Bioscience and Biotechnology, Tokyo Institute of Technology, Yokohama 226-8501, Japan

Supporting Information

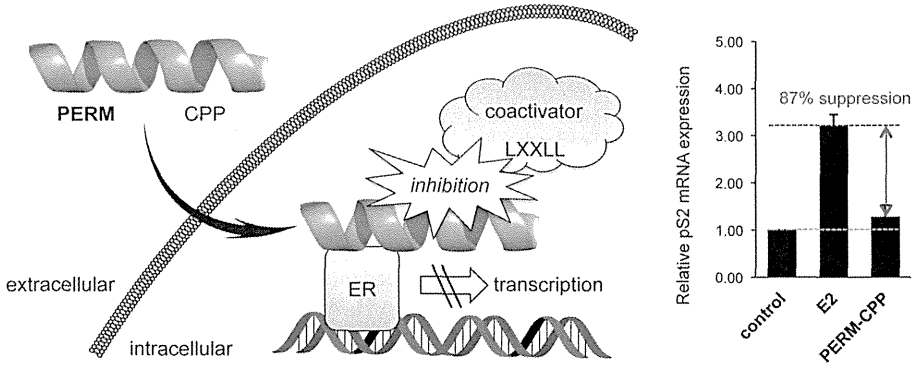

ABSTRACT: The heptaarginine (R7)-conjugated peptide **5** was designed and synthesized as an inhibitor of ER-coactivator interactions and ER-mediated transcription at the cellular level. The R7-conjugated peptide **5** was able to enter ER-positive T47D cells efficiently, and treatment with 3 μM of **5** downregulated the mRNA expression of pS2 (an ER-mediated gene) by 87%.

INTRODUCTION

Breast cancer is the most common cancer in women, and its incidence is increasing from year to year. The estrogen receptor (ER), which is a ligand-inducible transcription factor and a member of the nuclear receptor superfamily, is often overexpressed in the tissues of breast cancer patients and promotes the estrogen-dependent proliferation of cancer cells.[1−3] Several ERα antagonistic drugs, such as tamoxifen and nonsteroidal selective ER modulators, have been developed as treatments for breast cancer.[4−8] Among those antagonists, tamoxifen acts via the competitive inhibition of 17β-estradiol (E2) and is the most widely used drug for treating breast cancer.[9,10] However, tamoxifen has agonistic effects on ERα in uterine cancer cells and increases the risk of endometrial cancer.[11,12] In addition, it activates the protein kinase B (Akt) signaling pathway by binding to a particular ER variant, resulting in the inhibition of apoptosis in cancer cells.[13,14] Therefore, novel drug candidates with different mechanisms of action have long been desired. ER-mediated gene activation is induced by the binding of E2 to the ER ligand-binding domain and the subsequent binding of the consensus LXXLL helical motif[15] (L: leucine, X: any amino acid residue) of the coactivator with the ER surface.[16,17] Helical peptides containing the above-mentioned consensus sequence have been demonstrated to inhibit ER-coactivator interactions, and they are also considered to be drug candidates for reducing ER-mediated transactivation. Various helical peptides have been reported as inhibitors of ER-coactivator interactions.[18−22] The peptidomimetic estrogen receptor modulators (PERMs), specifically, PERM-1 and PERM-3 [with two mutation: Lys(1) → Arg(1) and Leu(7) → Npg(7)] reported by Burris et al. exhibited particularly potent inhibitory activity against ER-coactivator interactions.[19,20] However, only a few peptide-based ER-transcription inhibitors that exhibit potent activity at the cellular level have been reported[23,24] because of the low cell permeability of such peptides. Thus, we assumed that the conjugation of PERM with cell-penetrating peptides such as oligoarginines and their derivatives[25,26] might solve the problems surrounding the development of novel peptide-based transcriptional inhibitors (Figure 1). In this communication, we describe the synthesis of heptaarginine (R7)-conjugated PERM as inhibitors of ER-signaling at the cellular level (Table 1). Specifically, we synthesized R7-conjugated helical peptides and evaluated their cellular uptake, ability to inhibit transcription in ER-positive T47D cells, ability to inhibit ER-coactivator interactions, and their preferred secondary structures (by assessing their CD spectra).

RESULTS AND DISCUSSION

Synthesis of Peptides. The N-terminal-free peptides **1**−**7** and their N-terminal fluorescein (FAM) labeled peptides were

Received: October 17, 2014
Revised: November 5, 2014
Published: November 6, 2014

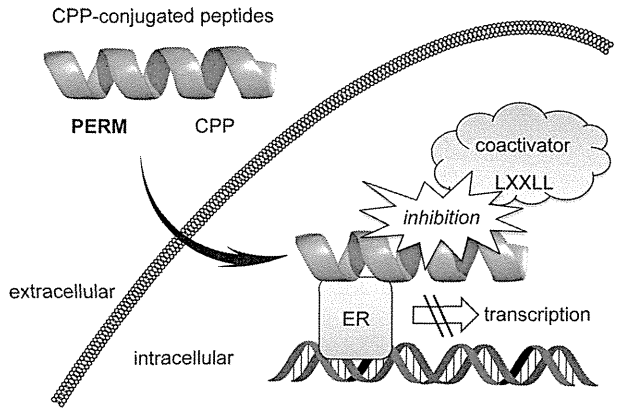

Figure 1. Illustration of the mechanism by which the CPP-conjugated peptides inhibited ER-coactivator interactions at the cellular level.

synthesized using microwave-assisted Fmoc-based solid phase methods, respectively. All of the peptides were purified by reversed-phase high performance liquid chromatography and were characterized using electrospray ionization time-of-flight mass spectrometry (Supporting Information).

Biological Evaluations. First of all, we evaluated the cellular uptake of fluorescein-labeled peptides (green; 1 μM) into ER-positive T47D cells (incubated for 3 h) using confocal laser scanning microscopy (CLSM, Supporting Information) as shown in Figure 2. The R7-unconjugated peptide **FAM-2** (an N-terminal fluorescein-labeled version of peptide **2**) was completely unable to enter the ER-positive T47D cells, whereas the R7-conjugated peptide **FAM-5** passed through the cell membrane efficiently and was distributed in the cytoplasm and nucleus. This difference in the cell-penetrating abilities of the molecules was solely due to the presence/absence of R7 conjugation. The R7-conjugated peptide **FAM-4** also exhibited cell permeability (Supporting Information).

Then, we evaluated the ability of the R7-conjugated peptides to inhibit ER-mediated transcription. Transcriptional analysis of an ER target gene (pS2) was carried out using T47D cells that had been incubated with one of the peptides (3 μM) in the absence or presence of 10 nM E2 for 24 h. The mRNA expression of pS2, which is the one gene whose expression is upregulated by E2, was analyzed using the quantitative polymerase chain reaction (Supporting Information). The relative pS2 mRNA expression levels of the cells treated with each peptide are summarized in Figure 3. The R7-unconjugated (nonmembrane-penetrating) peptides **1**–**3** and the heptaarginine (YR7)[27] peptide did not inhibit transcription. On the other hand, the mRNA expression of pS2 was significantly decreased (by 87%) by the addition of 3 μM of the R7-conjugated peptide **5**. Treatment with 3 μM of the R7-conjugated peptide **4** did not suppress the mRNA expression of pS2 at all, but treatment with 10 μM of **4** decreased it by 95% (Supporting Information). Conversely, treatment with the R7-conjugated peptide **6** at concentrations ranging from 3 μM to 10 μM did not induce any significant reduction in ER-mediated transcriptional activity. These results demonstrated that the R7-conjugated peptides **4** and **5** were able to exhibit antagonistic effects on ER-mediated transcription at the cellular level, and **5** displayed particularly potent inhibitory activity.

The inhibitory activity of peptides **4** and **5** against ER–coactivator interactions were evaluated using EnBio receptor cofactor assay systems (RCAS) for ERα (Fujikura Kasei Co., Ltd.) according to the manufacturer's instructions (Figure 4). The R7-unconjugated peptides **1** and **2** demonstrated strong activity against ERα–coactivator interactions. While the activities of the corresponding R7-conjugated peptides **4** and **5** were reduced, peptide **5** still demonstrated strong activity (IC_{50}: 94 nM). These results indicated that peptides **4** and **5** suppress ER-mediated transcription by inhibiting ERα–coactivator interactions. The R7-conjugated peptide **5** exhibited stronger inhibitory activity against ERα–coactivator interactions than **4**, and therefore, **5** was able to suppress ER-mediated transcription more efficiently than **4**, even at the cellular level.

The dominant conformations of peptides **1**–**6** were analyzed by assessing their CD spectra in 20% aqueous 2,2,2-trifluoroethanol (TFE) solution (Figure 5). The CD spectra of peptides **1** and **2**, and those of their R7-conjugated peptides **4** and **5**, displayed negative maxima at around 208 and 222 nm, indicating that all of the peptides formed stable right-handed α-helical structures. These findings suggested that the R7 fragment did not disrupt helix formation. On the other hand, the SRC-1 peptide **3** and its R7-conjugated form **6** were found to be composed of random coil structures rather than α-helices. These results indicated that peptides require stabilized helical structures in order to possess significant inhibitory activity against ER-coactivator interactions.

CONCLUSION

In conclusion, we developed heptaarginine (R7)-conjugated PERM as molecules that could be used to suppress ER-mediated transcription at the cellular level. The R7-conjugated peptides were able to enter ER-positive T47D cells efficiently, and one of them, peptide **5**, downregulated the mRNA expression of pS2 by 87% at a dose of 3 μM. Furthermore, **5** displayed strong inhibitory activity (IC_{50}: 94 nM) against ER–coactivator interactions. Although the inhibitory activity of the R7-conjugated peptide **5** against ER–coactivator interactions was slightly decreased compared with that of the R7-unconjugated peptide **2** (IC_{50}: 13 nM), **5** still exhibited potent activity. The dominant conformations of the peptides were analyzed based on

Table 1. Sequences of Peptides 1–7

peptide	sequence
PERM-1 (**1**)	H-Lys-*cyclo*(D-Cys-Ile-Leu-Cys)-Arg-Leu-Leu-Gln-NH_2
PERM-3 (**2**)	H-Arg-*cyclo*(D-Cys-Ile-Leu-Cys)-Arg-Npg[a]-Leu-Gln-NH_2
SRC-1[b] (**3**)	H-His-Lys-Ile-Leu-His-Arg-Leu-Leu-Gln-NH_2
PERM-1-R7 (**4**)	H-Lys-*cyclo*(D-Cys-Ile-Leu-Cys)-Arg-Leu-Leu-Gln-$(Gly)_3$-$(Arg)_7$-NH_2
PERM-3-R7 (**5**)	H-Arg-*cyclo*(D-Cys-Ile-Leu-Cys)-Arg-Npg-Leu-Gln-$(Gly)_3$-$(Arg)_7$-NH_2
SRC-1-R7 (**6**)	H-His-Lys-Ile-Leu-His-Arg-Leu-Leu-Gln-$(Gly)_3$-$(Arg)_7$-NH_2
YR7 (**7**)	H-Tyr-$(Arg)_7$-NH_2

[a]Npg: neopentylglycine. [b]The LXXLL motif of the coactivator.

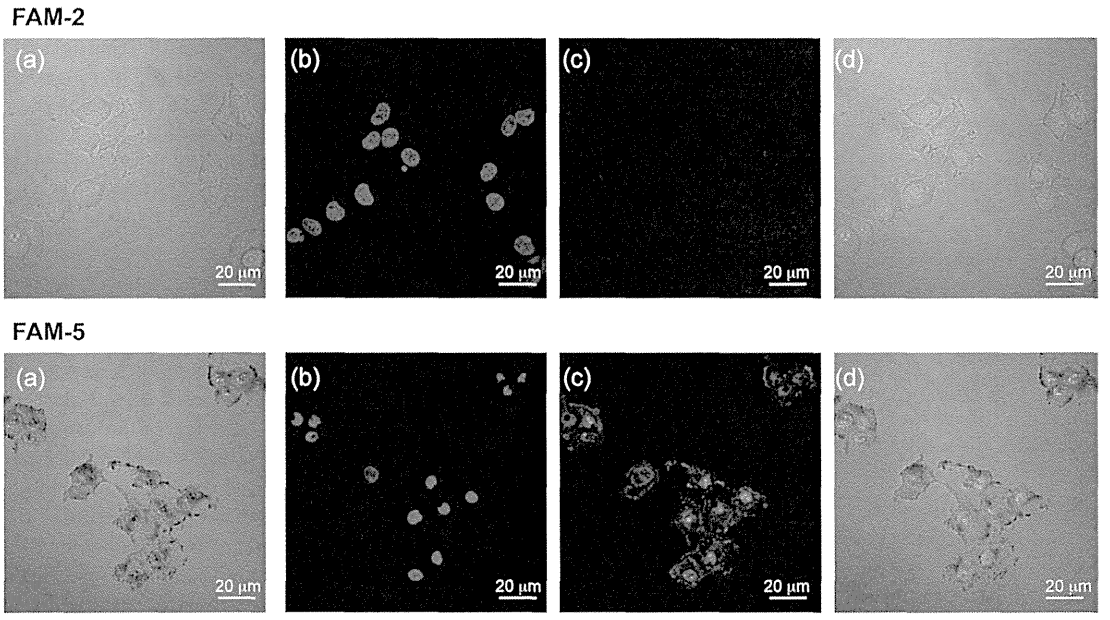

Figure 2. CLSM images of T47D cells that had been treated with **FAM-2** or **FAM-5** (peptide concentration: 1 μM, incubation time: 3 h). (a) Bright-field images, (b) nuclei stained with Hoechst 33342 (blue), (c) the intracellular distribution of the FAM-conjugated peptides (green), and (d) merged images.

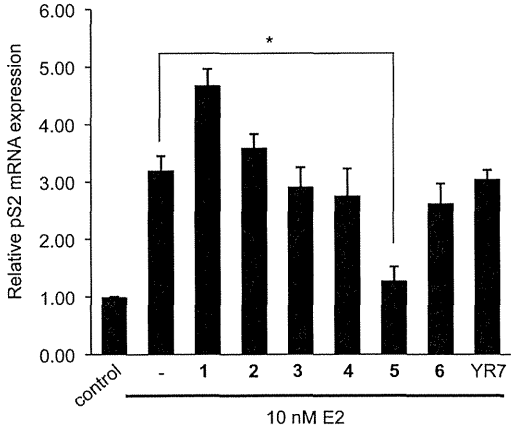

Figure 3. Inhibition of ERα-mediated gene expression in T47D cells. Peptide concentration: 3 μM. The error bars represent standard deviation, $n = 3$. *$p < 0.05$.

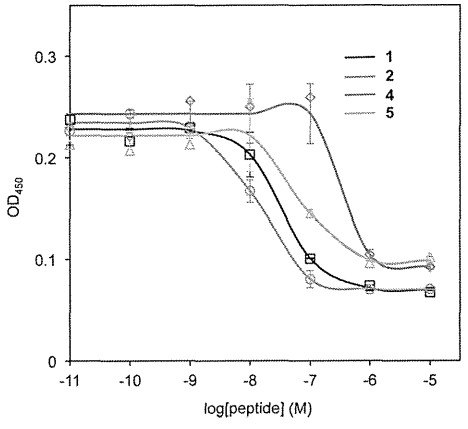

Peptide	IC_{50} (nM)
1	35
2	13
4	749
5	94

The EC_{50} value of the positive control, E2, was 1.5 nM.

Figure 4. IC_{50} values of peptides against ERα–cofactor interactions according to RCAS.

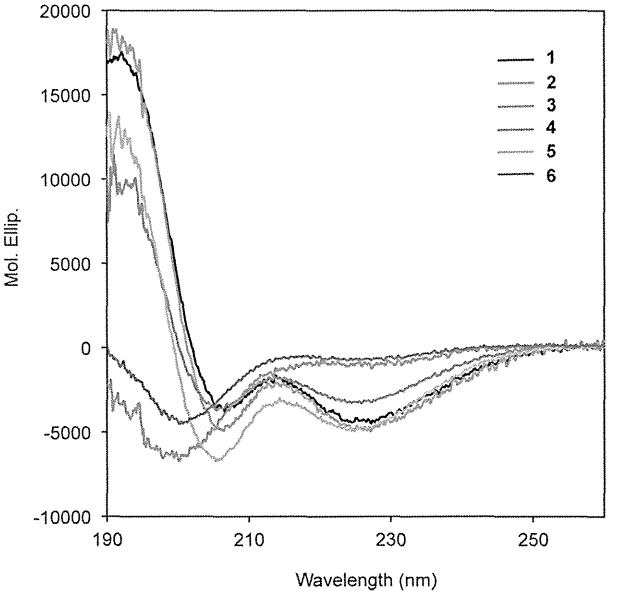

Figure 5. CD spectra of peptides **1**–**6** in the 190–260 nm region. Peptide concentration: 100 μM in 20% aqueous TFE solution.

their CD spectra, and it was found that **5** formed a right-handed α-helical structure similar to that of the R7-unconjugated peptide **2**. The R7-conjugation of the PERM did not disrupt their helical structures. These results indicate that the conjugation of PERM to R7 would aid the development of novel inhibitors of ER-mediated transcription at the cellular level. The derivatization of further helical peptides and detailed studies of their inhibitory mechanisms are currently underway.

■ ASSOCIATED CONTENT

Supporting Information

Information about the synthesis and purification of the peptides and the protocols of the in vitro assays. This material is available free of charge via the Internet at http://pubs.acs.org.

AUTHOR INFORMATION

Corresponding Authors

*E-mail: demizu@nihs.go.jp. Tel: + 81-3-3700-1141; Fax: + 81-3-3707-6950.

*E-mail: masaaki@nihs.go.jp. Tel: + 81-3-3700-1141; Fax: + 81-3-3707-6950.

Notes

The authors declare no competing financial interest.

ACKNOWLEDGMENTS

This study was supported, in part, by JSPS KAKENHI Grant Numbers 26460169 (Y.D.), 26670041 (Y.K.), and 25893038 (T.M.) and by a Grant-in-Aid from the Tokyo Biochemical Research Foundation (Y.D.).

ABBREVIATIONS

Akt, protein kinase B; CD, circular dichroism; CLSM, confocal laser scanning microscopy; ER, estrogen receptor; E2, 17β-estradiol; PERM, peptidomimetic estrogen receptor modulators; RCAS, receptor cofactor assay systems; R7, heptaarginine; TFE, 2,2,2-trifluoroethanol

REFERENCES

(1) Holst, F., Stahl, P. R., Ruiz, C., Hellwinkel, O., Jehan, Z., Wendland, M., Lebeau, A., Terracciano, L., Al-Kuraya, K., Jänicke, F., Sauter, G., and Simon, R. (2007) Estrogen receptor alpha (ESR1) gene amplification is frequent in breast cancer. *Nat. Genet. 39*, 655–660.

(2) Doisneau-Sixou, S. F., Cergio, C. M., Carroll, J. S., Hui, R., Musgrove, E. A., and Sutherland, R. L. (2003) Estrogen and antiestrogen regulation of cell cycle progression in breast cancer cells. *Endocrine-Related Cancer 10*, 179–186.

(3) Foster, J. S., Henley, D. C., Bukovsky, A., Seth, P., and Wimalasena, J. (2001) Multifaceted regulation of cell cycle progression by estrogen: regulation of Cdk inhibitors and Cdc25A independent of cyclin D1-Cdk4 function. *Mol. Cell. Biol. 21*, 794–810.

(4) Howell, S. J., Johnston, S. R., and Howell, A. (2004) The use of selective estrogen receptor modulators and selective estrogen receptor down-regulators in breast cancer. *Best Pract. Res. Clin. Endocrinol. Metab. 18*, 47–66.

(5) Deroo, B. J., and Korach, K. S. (2006) Estrogen receptors and human disease. *J. Clin. Invest. 116*, 561–570.

(6) Baumann, C. K., and Castiglione-Gertsch, M. (2007) Estrogen receptor modulators and down regulators. *Drugs 67*, 2335–2353.

(7) Demizu, Y., Okuhira, H., Motoi, H., Ohno, A., Shoda, T., Fukuhara, K., Okuda, H., Naito, M., and Kurihara, M. (2012) Design and synthesis of estrogen receptor degradation inducer based on a protein knockdown strategy. *Bioorg. Med. Chem. Lett. 22*, 1793–1796.

(8) Shoda, T., Okuhira, K., Kato, M., Demizu, Y., Inoue, H., Naito, M., and Kurihara, M. (2014) Design and synthesis of tamoxifen derivatives as a selective estrogen receptor down-regulator. *Bioorg. Med. Chem. Lett. 24*, 87–89.

(9) Early Breast Cancer Trialists' Collaborative Group (1992) Systemic treatment of early breast cancer by hormonal, cytotoxic, or immune therapy: 133 randomised trials involving 31 000 recurrences and 24 000 deaths among 75 000 women. *Lancet 339*, 71–85.

(10) Fisher, B., Costantino, J. P., Wickerham, D. L., Redmond, C. K., Kavanah, M., Cronin, W. M., Vogel, V., Robidoux, A., Dimitrov, N., Atkins, J., Daly, M., Wieand, S., Tan-Chiu, E., Ford, L., and Wolmark, N. (1998) Tamoxifen for prevention of breast cancer: Report of the national surgical adjuvant breast and bowel project P-1 study. *J. Natl. Cancer Inst. (Bethesda) 90*, 1371–1388.

(11) Bernstein, L., Deapen, D., Cerhan, J. R., Schwartz, S. M., Liff, J., McGann-Maloney, E., Perlman, J. A., and Ford, L. (1999) Tamoxifen therapy for breast cancer and endometrial cancer risk. *J. Natl. Cancer Inst. 91*, 1654–1662.

(12) Shang, Y., and Brown, M. (2002) Molecular determinants for the tissue specificity of SERMs. *Science 295*, 2465–2468.

(13) Arpino, G., Wiechmann, L., Osborne, C. K., and Schiff, R. (2008) Crosstalk between the estrogen receptor and the HER tyrosine kinase receptor family: molecular mechanism and clinical implications for endocrine therapy resistance. *Endocr. Rev. 29*, 217–233.

(14) Lin, S.-L., Yan, L.-Y., Zhang, X.-T., Yuan, J., Li, M., Qiao, J., Wang, Z.-Y., Sheng, J., and Sun, Q.-Y. (2010) ER-alpha36, a variant of ER-alpha, promotes tamoxifen agonist action in endometrial cancer cells via the MAPK/ERK and PI3K/Akt pathways. *PLoS One 5*, e9013.

(15) Demizu, Y., Nagoya, S., Shirakawa, M., Kawamura, M., Yamagata, N., Sato, Y., Doi, M., and Kurihara, M. (2013) Development of stapled short helical peptides capable of inhibiting vitamin D receptor (VDR)-coactivator interactions. *Bioorg. Med. Chem. Lett. 23*, 4292–4296.

(16) Heery, D. M., Kalkhoven, E., Hoare, S., and Parker, M. G. (1997) A signature motif in transcriptional co-activators mediates binding to nuclear receptors. *Nature 387*, 733–736.

(17) Hall, J. M., and McDonnell, D. P. (2005) Coregulators in nuclear estrogen receptor action: from concept to therapeutic targeting. *Mol. Interventions 5*, 343–357.

(18) Hall, J. M., Chang, C., and McDonnell, D. P. (2000) Development of peptide antagonists that target estrogen receptorβ-coactivator interactions. *Mol. Endocrinol. 14*, 2010–2023.

(19) Leduc, A.-M., Trent, J. O., Wittliff, J. L., Bramlett, K. S., Briggs, S. L., Chirgadze, N. Y., Wang, Y., Burris, T. P., and Spatola, A. F. (2003) Helix-stabilized cyclic peptides as selective inhibitors of steroid receptor-coactivator interactions. *Proc. Natl. Acad. Sci. U.S.A. 100*, 11273–11278.

(20) Galande, A. K., Bramlett, K. S., Trent, J. O., Burris, T. P., Wittliff, J. L., and Spatola, A. F. (2005) Protein inhibitors of LXXLL-based protein-protein interactions. *ChemBioChem 6*, 1991–1998.

(21) Phan, T., Nguyen, H. D., Göksel, H., Möcklinghoff, S., and Brunsveld, L. (2010) Phage display selection of miniprotein binders of the Estrogen receptor. *Chem. Commun. 46*, 8207–8209.

(22) Phillips, C., Roberts, L. R., Schade, M., Bazin, R., Bent, A., Davies, N. L., Moore, R., Pannifer, A. D., Pickford, A. R., Prior, S. H., Read, C. M., Scott, A., Brown, D. G., Xu, B., and Irving, S. L. (2011) Design and structure of stapled peptides binding to estrogen receptors. *J. Am. Chem. Soc. 46*, 8207–8209.

(23) Carraz, M., Zwart, W., Phan, T., Michalides, R., and Brunsveld, L. (2009) Perturbation of estrogen receptor α localization with synthetic nona-arginine LXXLL-peptide coactivator binding inhibitors. *Chem. Biol. 16*, 702–711.

(24) Tints, K., Prink, M., Neuman, T., and Palm, K. (2014) LXXLL peptide converts transportan 10 to a potent inducer of apoptosis in breast cancer cells. *Int. J. Mol. Sci. 15*, 5680–5698.

(25) Nakase, I., Akita, H., Kogure, K., Gräslund, A., Langel, Ü., Harashima, H., and Futaki, S. (2012) Efficient intracellular delivery of nucleic acid pharmaceuticals using cell-penetrating peptides. *Acc. Chem. Res. 45*, 1132–1139.

(26) Yamashita, H., Demizu, Y., Shoda, T., Sato, Y., Oba, M., Tanaka, M., and Kurihara, M. (2014) Amphipathic short helix-stabilized peptides with cell-membrane penetrating ability. *Bioorg. Med. Chem. 22*, 2403–2408.

(27) A tyrosine residue was attached to the N-terminus of the heptaarginine fragment, as it enabled the concentrations of the peptides to be determined.

nature COMMUNICATIONS

ARTICLE

Received 28 Dec 2013 | Accepted 25 Jul 2014 | Published 25 Sep 2014

DOI: 10.1038/ncomms5806

Sphingosine-1-phosphate promotes expansion of cancer stem cells via S1PR3 by a ligand-independent Notch activation

Naoya Hirata[1], Shigeru Yamada[1], Takuji Shoda[2], Masaaki Kurihara[2], Yuko Sekino[1] & Yasunari Kanda[1]

Many tumours originate from cancer stem cells (CSCs), which is a small population of cells that display stem cell properties. However, the molecular mechanisms that regulate CSC frequency remain poorly understood. Here, using microarray screening in aldehyde dehydrogenase (ALDH)-positive CSC model, we identify a fundamental role for a lipid mediator sphingosine-1-phosphate (S1P) in CSC expansion. Stimulation with S1P enhances ALDH-positive CSCs via S1P receptor 3 (S1PR3) and subsequent Notch activation. CSCs overexpressing sphingosine kinase 1 (SphK1), an S1P-producing enzyme, show increased ability to develop tumours in nude mice, compared with parent cells or CSCs. Tumorigenicity of CSCs overexpressing SphK1 is inhibited by *S1PR3* knockdown or S1PR3 antagonist. Breast cancer patient-derived mammospheres contain SphK1$^+$/ALDH1$^+$ cells or S1PR3$^+$/ALDH1$^+$ cells. Our findings provide new insights into the lipid-mediated regulation of CSCs via Notch signalling, and rationale for targeting S1PR3 in cancer.

[1] Division of Pharmacology, National Institute of Health Sciences, Setagaya-ku, Tokyo 158-8501, Japan. [2] Division of Organic Chemistry, National Institute of Health Sciences, Setagaya-ku, Tokyo 158-8501, Japan. Correspondence and requests for materials should be addressed to Y.K. (email: kanda@nihs.go.jp).

Growing evidence suggests that many types of cancer, including breast, lung and prostate cancer, are initiated from a small population of cancer stem cells (CSCs; also called tumour-initiating cells)[1–8]. This minor population produces the bulk of cancers through continuous self-renewal and differentiation, which contributes to cancer heterogeneity. Therefore, it is essential to elucidate the signalling and regulatory mechanisms that are unique to CSCs, and to design novel therapeutic agents against CSCs.

CSCs have been isolated from diverse tumours and established cell lines, using several methods encompassing cell surface markers, aldehyde dehydrogenase (ALDH) activity, side population (SP) and sphere-forming ability. ALDH assays rely on the fact that the level of ALDH, a detoxifying enzyme responsible for the oxidation of intracellular aldehydes, is higher in stem cells than in differentiated cells[4]. ALDH1 expression is correlated with poor clinical prognosis in various cancers, such as breast, lung and prostate cancer[4–6]. Because CSCs have been considered to have molecular similarities to embryonic and normal adult stem cells, the self-renewal behaviour of CSCs has been reported to be mediated by several signalling pathways, such as Notch, Hedgehog and Wnt[9]. However, the molecular mechanisms that regulate the frequency and maintenance of CSCs via self-renewal signals remain poorly understood.

Autocrine and paracrine signalling plays a key role in maintaining the stem cell state and expansion of stem cells[10]. We therefore speculated that receptors for autocrine/paracrine factors might play a key role in CSC regulation. Using microarray screening in an ALDH-positive cell population of human breast cancer MCF-7 cells, we found that several receptors are upregulated. Among them, on the basis of pathophysiological properties, we focused on S1P receptor 3 (S1PR3), a receptor for a lipid mediator sphingosine-1-phospahate (S1P). S1P is known to exert multiple responses, such as proliferation, survival and cytoskeletal rearrangement, via its G protein-coupled receptor (GPCR) in many cell types[11]. S1P is synthesized from sphingosine by sphingosine kinase (SphK); two isoforms of mammalian SphK (sphingosine kinase 1 (SphK1) and SphK2) have been cloned and characterized[12,13]. In addition, the SphK1/S1P pathway has also been implicated in tumour progression[14,15]. S1P has also been shown to accumulate in the tumour microenvironment[16]. Although lipid mediators in cancer have been studied extensively, the role(s) of SphK1/S1P in CSCs remain unclear.

We demonstrate here that S1P regulates expansion of CSCs in several types of cancer. Our findings suggest that Notch activation is essential for S1P-induced proliferation of CSCs via S1PR3. We show that SphK1 regulates the tumorigenicity of breast CSCs via S1PR3. Using clinical samples, we show that breast cancer patient-derived CSCs contain SphK1$^+$/ALDH1$^+$ cells or S1PR3$^+$/ALDH1$^+$ cells. Thus, these results implicate the S1P signalling pathway as therapeutic targets in CSCs.

Results

S1P is a regulator of CSC population via S1PR3. We used an ALDH assay system to study the signalling pathways that regulate the frequency and maintenance of CSCs. Many cancer cell lines, including oestrogen receptor-positive MCF-7 cells, are known to contain an ALDH-positive cell population[5,6,17,18]. Consistent with a previous report[4], we confirmed that ALDH-positive cell population in MCF-7 cells possessed CSC-like properties, as assessed by expression of stem cell markers, drug resistance and tumorigenicity (Supplementary Fig. 1). Through microarray analysis, we investigated a possible receptor that increases the proportion of the ALDH-positive cell population in MCF-7 cells as a CSC model. We found *S1PR3* as a possible candidate in CSC regulation (Supplementary Data 1). *S1PR3* was highly expressed in the ALDH-positive cell population, a finding confirmed by quantitative polymerase chain reaction (qPCR) assays (Fig. 1a). *S1PR2* expression was lower in the ALDH-positive cell population compared with MCF-7 cells, and other types of *S1PR* are yet to be detected in MCF-7 cells (Supplementary Fig. 2)[19,20]. Stimulation with S1P increased the proportion of ALDH-positive cell population in a dose-dependent manner, with a maximal response observed at 100 nM (Fig. 1b). Similar to S1P, dihydro-S1P, another S1PR3 ligand, also increased the ALDH-positive cell population (Supplementary Fig. 3). Moreover, stimulation with S1P increased the number of SP cells (Fig. 1c), mammosphere-forming efficiency (Fig. 1d), CD44$^+$/CD24$^-$ population (Fig. 1e) and expression of stem cell markers (Fig. 1f). These data indicate that stimulation with S1P leads to an increase in breast CSCs. In contrast, lysophosphatidic acid (LPA), another well-studied lipid mediator, did not increase CSCs in MCF-7 cells. To confirm the involvement of S1PR3, we inhibited S1PR3 using pharmacological antagonists and RNA interference techniques. The effects of S1P were blocked by the S1PR3 antagonist TY52156 (ref. 21). Another antagonist CAY10444, which is structurally different from TY52156, also inhibited the S1P effect. In contrast, the S1PR2 antagonist JTE013 had little effect (Fig. 1g). Experiments using small interfering RNAs (siRNA) confirmed the effects of antagonists (Fig. 1h). In addition, short hairpin RNAs (shRNAs) against *S1PR3* also inhibited the enhancement of mammosphere-forming ability by S1P (Supplementary Fig.4). Similar results with ALDH assay were obtained in triple-negative MDA-MB-231 cells (Supplementary Fig. 5a,b), suggesting that S1P regulates both luminal and triple-negative type of breast CSCs. Furthermore, we examined CSCs from other tumour types to determine whether these effects of S1P are limited to breast cancer cell lines. Similar to MCF-7 cells, stimulation with S1P increased the ALDH-positive cell population in human lung cancer A549 cells, human prostate cancer LNCaP cells, human glioma U251MG cells and human ovarian cancer OVCAR-5 cells (Supplementary Fig. 6a). In addition, TY52156 inhibited the S1P effect in these cell lines. Taken together, these data demonstrate that S1P has an ability to increase the number of CSCs via S1PR3 in several types of cancer.

S1P enhances Notch signalling via S1PR3. Growing evidence suggests many similarities between embryonic stem cells and CSCs[9]; therefore, we focused on Notch, Hedgehog and Wnt as signalling pathway candidates downstream of the S1PR. Stimulation with S1P induced expression of the Notch target gene *Hes1* in MCF-7 cells (Fig. 2a) and ALDH-positive MCF-7 cells (Supplementary Fig. 7a). Moreover, S1P also induced the *Hes1* expression in ALDH-positive A549, LNCaP, U251 and OVCAR-5 cells (Supplementary Fig. 7b). S1P-induced *Hes1* expression was inhibited by S1PR3 antagonists (Fig. 2b). In contrast, the Hedgehog target gene *Gli1*, and Wnt target gene *Dkk1* were not induced. The effect of S1P on ALDH-positive cell population was inhibited by DAPT, an inhibitor of γ-secretase, which has multiple substrates including Notch, not by the Hedgehog inhibitor cyclopamine and the Wnt inhibitor PNU74654 (Fig. 2c; Supplementary Fig. 8). Similar effects of DAPT were obtained in MDA-MB-231 cells (Supplementary Fig. 5d), A549 cells, LNCaP cells, U251 cells and OVCAR-5 cells (Supplementary Fig. 6b). To determine whether S1P has the ability to activate the Notch pathway, we examined cleavage of Notch in MCF-7 cells. Stimulation with S1P produced the Notch intracellular domain (N1ICD) (Fig. 2d) and induced activation of the Notch transcriptional reporter *CSL*-luc (Fig. 2e). Because *Hes1* expression is dependent on NICD/CSL/MAML

complex-mediated gene transcription[22], we verified whether co-activators were involved in CSCs, using dominant-negative (DN) mutants of CSL, which have been reported to have no ability to bind to DNA[23]. DN-CSL inhibited S1P-induced *Hes1* expression and the ALDH-positive cell population (Fig. 2f). Similar results were obtained by DN-MAML, which lacks transcriptional activating domain and inhibits NICD-dependent transcriptional activition[24]. To examine which subtype of Notch was involved in CSCs, we overexpressed each type of NICD. Overexpression of N1ICD increased *Hes1* expression and the ALDH-positive cell population (Fig. 2g). N3ICD also increased the ALDH-positive cell population (Supplementary Fig. 9a), while N2ICD and

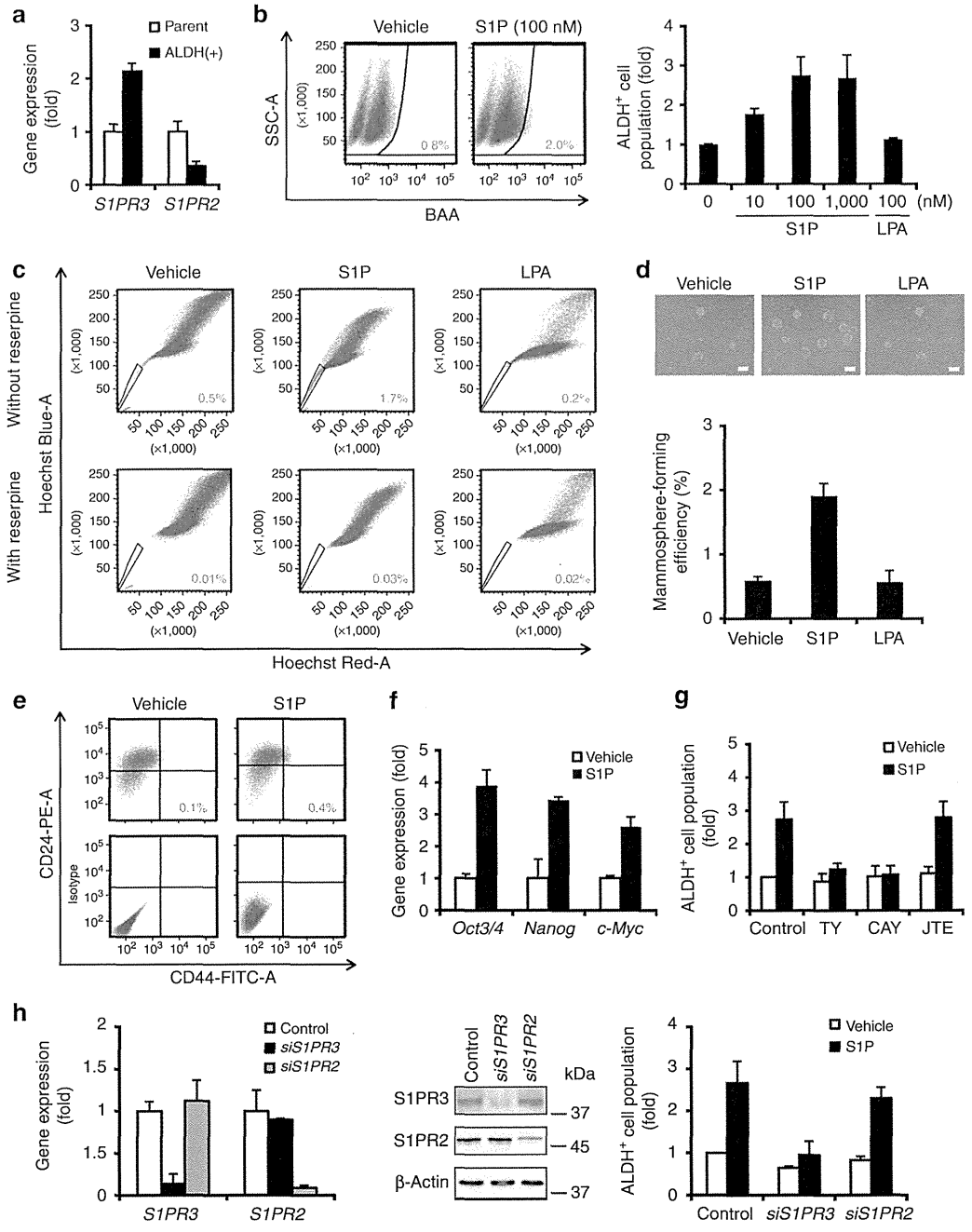

Figure 1 | Role of S1PR3 in the ALDH-positive cell population within the MCF-7 cell line. (**a**) Expression levels of S1PR (*S1PR2* and *S1PR3*) in parental or ALDH-positive MCF-7 cells by qPCR. Data represent mean ± s.d. ($n=3$). (**b**) Representative flow data with ALDH substrate in the presence or absence of S1P (100 nM, 3 days) in MCF-7 cells. Dose-dependent effects of S1P in the proportion of ALDH-positive cell population. Data represent mean ± s.d. ($n=3$). (**c**) Representative flow data of the SP assay with Hoechst 33342 dye alone or in the presence of reserpine (15 μg ml^{-1}). (**d**) Effects of S1P (100 nM) on mammosphere-forming efficiency in MCF-7 cells. The number of mammospheres was microscopically counted and the percentage of mammosphere-forming cells was determined as mammosphere-forming efficiency (%). The scale bar, 100 μm. Data represent mean ± s.d. ($n=3$). (**e**) Effects of S1P (100 nM) on CD44$^+$/CD24$^-$ population in MCF-7 cells. (**f**) Effects of S1P (100 nM) on expression of stem cell markers by qPCR. Data represent mean ± s.d. ($n=3$). (**g**) Effects of S1PR3 antagonists (TY52156, 1 μM; CAY10444, 10 μM) and the S1PR2 antagonist (JTE013, 10 μM) on S1P-induced increase in the ALDH-positive cell population. Data represent mean ± s.d. ($n=3$). (**h**) After transfection with siRNA, expression levels of S1P receptor were examined by qPCR and immunoblotting. Effects of siRNAs against *S1PR3* and *S1PR2* on S1P-induced increase in the ALDH-positive cell population. Data represent mean ± s.d. ($n=3$). Expression levels were normalized to glyceraldehyde 3-phosphate dehydrogenase messenger RNAs.

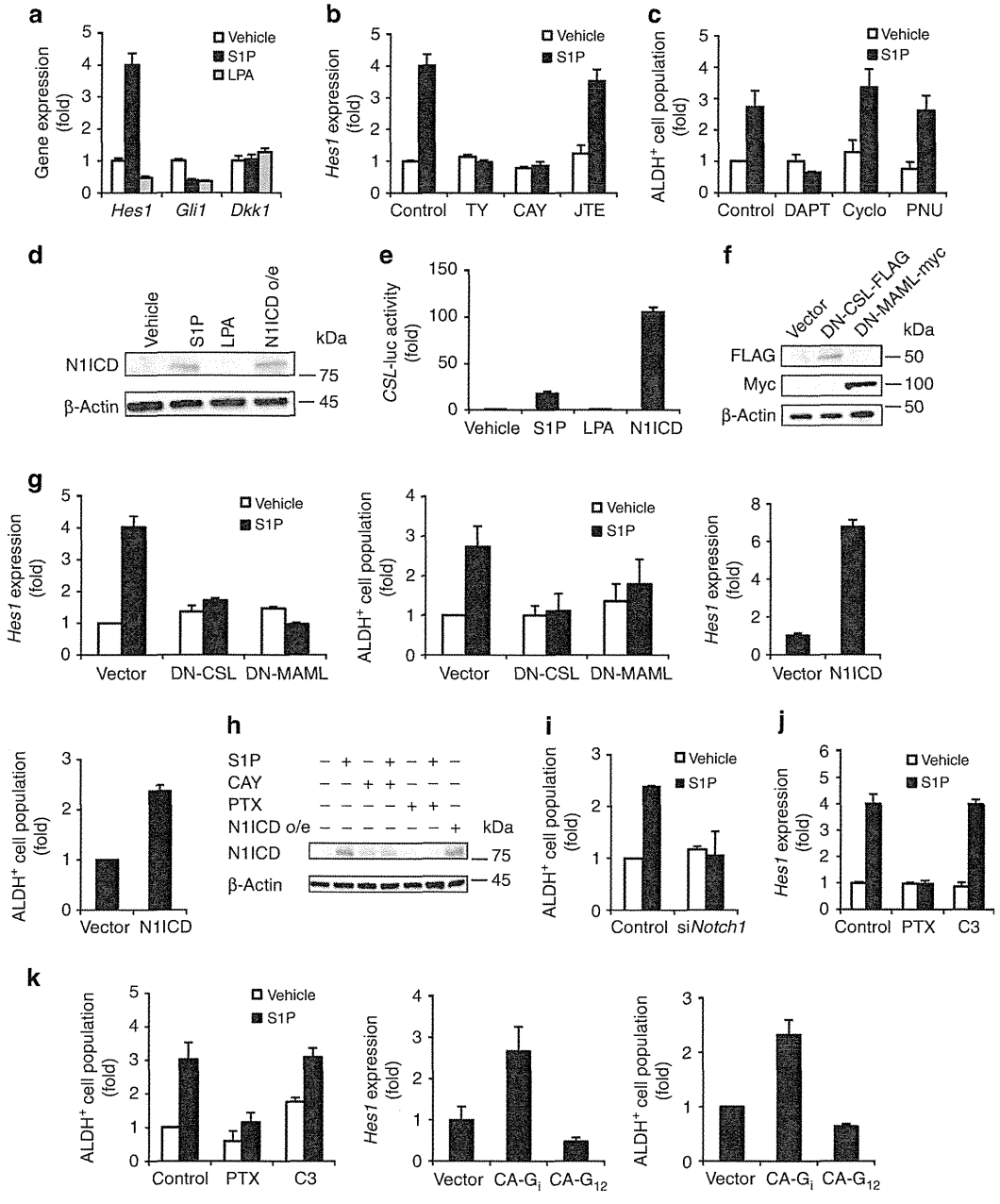

Figure 2 | Role of Notch signalling in ALDH-positive cell population. (**a**) After stimulation with S1P (100 nM) or LPA (100 nM) for 24 h, expression levels of the Notch target gene (*Hes1*), Hedgehog target gene (*Gli1*) and Wnt target gene (*Dkk1*) were quantified in MCF-7 cells using qPCR. Data represent mean ± s.d. ($n=3$). (**b**) Effects of TY52156 (1 μM) or CAY10444 (10 μM) on S1P-induced *Hes1* expression using qPCR. Data represent mean ± s.d. ($n=3$). (**c**) Effects of the Notch inhibitor DAPT (5 μM), the Hedgehog inhibitor cyclopamine (10 μM) or the Wnt inhibitor PNU74654 (10 μM) on S1P-induced increase in the ALDH-positive cell population. Data represent mean ± s.d. ($n=3$). (**d**) Effects of S1P or LPA on N1ICD production by immunoblotting. (**e**) MCF-7 cells transfected with a reporter plasmid encoding CSL-luc were cultured with or without S1P or LPA and were then analysed by luciferase assays. Data represent mean ± s.d. ($n=3$). (**f**) Effects of overexpression of Flag-tagged DN-CSL or myc-tagged DN-MAML on S1P-induced *Hes1* expression and ALDH-positive cell population. Data represent mean ± s.d. ($n=3$). The expression of plasmids was analysed by immunoblotting using tag-specific antibodies. (**g**) Effects of overexpression of N1ICD on *Hes1* expression and ALDH-positive cell population. Data represent mean ± s.d. ($n=3$). (**h**) After pretreatment with PTX (0.1 μg ml^{-1}, 24 h) or CAY10444 (10 μM, 30 min), the cells were stimulated with S1P. N1ICD production was analysed by immunoblotting with N1ICD-specific antibodies. (**i**) Effects of siRNA against *Notch1* on S1P-induced increase in the ALDH-positive cell population. Data represent mean ± s.d. ($n=3$). (**j**) Effects of toxins (PTX, 0.1 μg ml^{-1}; C3 Toxin, 0.1 μg ml^{-1}) on S1P-induced *Hes1* expression and ALDH-positive cell population. Data represent mean ± s.d. ($n=3$). (**k**) Effects of overexpression of CA mutants of G_i or G_{12} on S1P-induced *Hes1* expression and ALDH-positive cell population. Data represent mean ± s.d. ($n=3$). Expression levels were normalized to glyceraldehyde 3-phosphate dehydrogenase messenger RNAs.

N4ICD had little effect. S1P-induced N1ICD production was inhibited by CAY10444 (Fig. 2h); however, S1P did not induce N3ICD production (Supplementary Fig. 9b). To further examine the involvement of Notch in CSC, we performed knockdown experiments using *Notch1* siRNA. Knockdown of *Notch1* inhibited the effect of S1P on ALDH-positive cell population (Fig. 2i; Supplementary Fig. 10). Taken together, these data suggest crosstalk between S1P and Notch1. To confirm the

involvement of S1PR3 in crosstalk, we studied subtype of G proteins coupled to S1PR3. Pertussis toxin (PTX), which inactivates G_i protein, abolished S1P-induced *Hes1* expression and the ALDH-positive cell population, whereas C3 toxin, which inactivates an effector of $G_{12/13}$ Rho, had little effect (Fig. 2j). The effects of toxins were confirmed by overexpression of constitutively active (CA) mutants for G_i, but not by CA-G_{12} (Fig. 2k). These data suggest that G_i mediates S1P-induced Notch activation via S1PR3. Collectively, S1P has an ability to increase the number of CSCs via Notch signalling in several types of cancer.

S1P increases ADAM17 activity without Notch ligands. We further investigated the molecular mechanism of crosstalk between S1P and Notch in MCF-7 cells. Notch is generally activated by binding of Notch ligands to Notch and then cleaved by ADAM17 and γ-secretase[25]. Among Notch ligands (Jagged1, 2 and Delta-like ligand (Dll) 1, 3 and 4), Dll3 is not capable to activate Notch signalling in adjacent cells[26].

To examine whether Notch ligands are required for the S1P effect, we examined the expression level of Notch ligands. S1P did not induce expression levels of Notch ligands (Supplementary Fig. 11a). Knockdown of Notch ligands did not affect S1P-induced *Hes1* expression and ALDH-positive cell population (Fig. 3a,b). In contrast to S1P, knockdown of Notch ligands inhibited hypoxia-mimetic agent desferoxamine-induced *Hes1* expression. In addition, neutralizing antibodies to Jagged1 inhibited *Hes1* induction by soluble Jagged1-Fc, but not S1P-induced *Hes1* expression and ALDH-positive cell population (Supplementary Fig. 11c,d). Taken together, these data suggest that S1P activates Notch signalling in Notch ligand-independent manner.

We next studied cleavage enzymes that are responsible for S1P-induced Notch activation. We found that stimulation with S1P increased ADAM17 activity in MCF-7 cells (Fig. 3c) and ALDH-positive MCF-7 cells (Supplementary Fig. 7c). In addition, S1P also increased γ-secretase activity in MCF-7 cells (Supplementary Fig. 12a). CAY10444 and PTX inhibited S1P-induced ADAM17 activation (Fig. 3d) and γ-secretase activation (Supplementary Fig. 12b). Overexpression of CA-G_i also increased both ADAM17 (Fig. 3e) and γ-secretase activity (Supplementary Fig. 12c). Moreover, we examined whether ADAM17 activation occurred in CSCs. Overexpression of ADAM17 increased N1ICD production, *Hes1* expression and the ALDH-positive cell population (Fig. 3f). Conversely, DN-ADAM17 (E406A; point mutation at metalloprotease domain)[27] inhibited S1P-induced responses (Fig. 3g). Expression of ADAM10 or DN-ADAM10 (E384A; point mutation at metalloprotease domain)[28] had little effect on the CSC signalling pathway. These data suggest that ADAM17 is involved in S1P-induced CSC proliferation.

p38MAPK mediates ADAM17 activation by S1P. We investigated whether the intracellular domain of ADAM17 plays a role in S1P-induced breast CSC proliferation. ADAM17 activity is regulated by phosphorylation-dependent mechanisms[29–31]; therefore, we generated ADAM17 mutants with either Thr735 (p38MAPK consensus motif) or Thr761 (Akt consensus motif) replaced by alanine (Fig. 4a). Consistent with our data above, S1P induced ADAM17 phosphorylation at Thr735 (Fig. 4b). S1P-induced ADAM17 phosphorylation was inhibited by PTX and CAY10444. A mutation at Thr735 decreased ADAM17 phosphorylation through S1P, whereas a mutation at Thr761 had little effect (Fig. 4c). In addition, mutation of Thr735 inhibited S1P-induced ADAM17 activation, *Hes1* expression and the number of ALDH-positive cell population (Fig. 4d). To further confirm the involvement of p38MAPK, we studied the association between p38MAPK and ADAM17. Stimulation with S1P induced a transient phosphorylation of p38MAPK (Supplementary Fig. 13a) and an association between p38MAPK and ADAM17 (Fig. 4e). Mutation of Thr735 abolished this association (Fig. 4f), suggesting that phospho-p38MAPK binds to ADAM17 at Thr735. Treatment with CAY10444 or PTX also inhibited the S1P-induced association between p38MAPK and ADAM17 (Fig. 4g). The p38MAPK inhibitor SB203580 inhibited the S1P-induced responses (Supplementary Fig. 13b–d). Furthermore, SB203580 inhibited the association between p38MAPK and ADAM17 (Supplementary Fig. 13f). In contrast, the PI3-kinase/Akt pathway inhibitor LY294002 had little effect (Supplementary Fig. 13b–e). Taken together, these data suggest that p38MAPK-mediated ADAM17 activation is involved in the S1P-induced CSC phenotype.

SphK1 increases CSCs via S1PR3. S1P is synthesized through SphK-catalyzed phosphorylation of sphingosine[11,14]. We next examined whether SphK is involved in breast CSCs. Consistent with previous reports[32,33], overexpressed SphK1 was localized in the cytosol, and SphK2 was mainly localized to the nucleus (Fig. 5a). Enzyme activities of SphKs were also confirmed (Supplementary Fig. 14). Overexpression of SphK1 increased the number of ALDH-positive cell population in both MCF-7 (Fig. 5b) and MDA-MB-231 cells (Supplementary Fig. 15), whereas SphK2 had little effect. Consistent with the ALDH assay results, ADAM17 activation, N1ICD production and *Hes1* expression were induced by SphK1 but not SphK2 (Fig. 5c). To determine whether intracellular S1P is involved in the SphK1 effect, we tested the effects of the S1PR3 antagonist on SphK1-induced increases in the ALDH-positive cell population. Pretreatment with CAY10444 inhibited SphK1-induced responses (Fig. 5d). *S1PR3* shRNAs also inhibited these SphK1-induced responses (Fig. 5e). Analysis by qPCR confirmed specific suppression of *S1PR3* by these shRNAs (Fig. 5e), and treatment with PTX also produced similar results. Recent studies suggest that the ABC transporter mediates oestrogen-induced S1P secretion in MCF-7 cells[34]. To determine whether the ABC transporter is involved with the SphK1 effect, we used siRNAs and a selective inhibitor to inhibit the transporter. An siRNA against *ABCC1* inhibited SphK1-induced ADAM17 activation, *Hes1* expression and the ALDH-positive cell population (Supplementary Fig. 16a). The ABCC1 inhibitor MK571 also produced similar results (Supplementary Fig. 16b). In contrast, an siRNA against *Spns2*, another S1P transporter[35], had little effects. These data suggest that S1P produced by SphK1 stimulates S1PR3, and leads to an increase in the number of CSCs.

SphK1 accelerates tumour formation of CSCs via S1PR3. Since S1P is easily degraded by S1P lyase or phosphatases, we next studied tumorigenicity using SphK1- or SphK2-overexpressing CSCs in MCF-7 cells. Almost all nude mice injected with SphK1-overexpressing ALDH-positive cells developed tumours within 6 weeks. Tumour formation was inefficient in the mice injected with vector- or SphK2-overexpressing ALDH-positive cells (Fig. 6a,b). Tumour sizes from SphK1-overexpressing ALDH-positive cells were bigger than those from vector- or SphK2-overexpressing ALDH-positive cells (Fig. 6c,d). Histological analysis indicated that tumours derived from the ALDH-positive cells and the SphK1-overexpressing ALDH-positive cells had similar morphologies (Fig. 6e). To examine the proportion of ALDH-positive cells in xenografted tumour samples, we conducted double staining using ALDH assays and human-specific antibodies to TRA-1-85 (Supplementary Fig. 17). The increase in

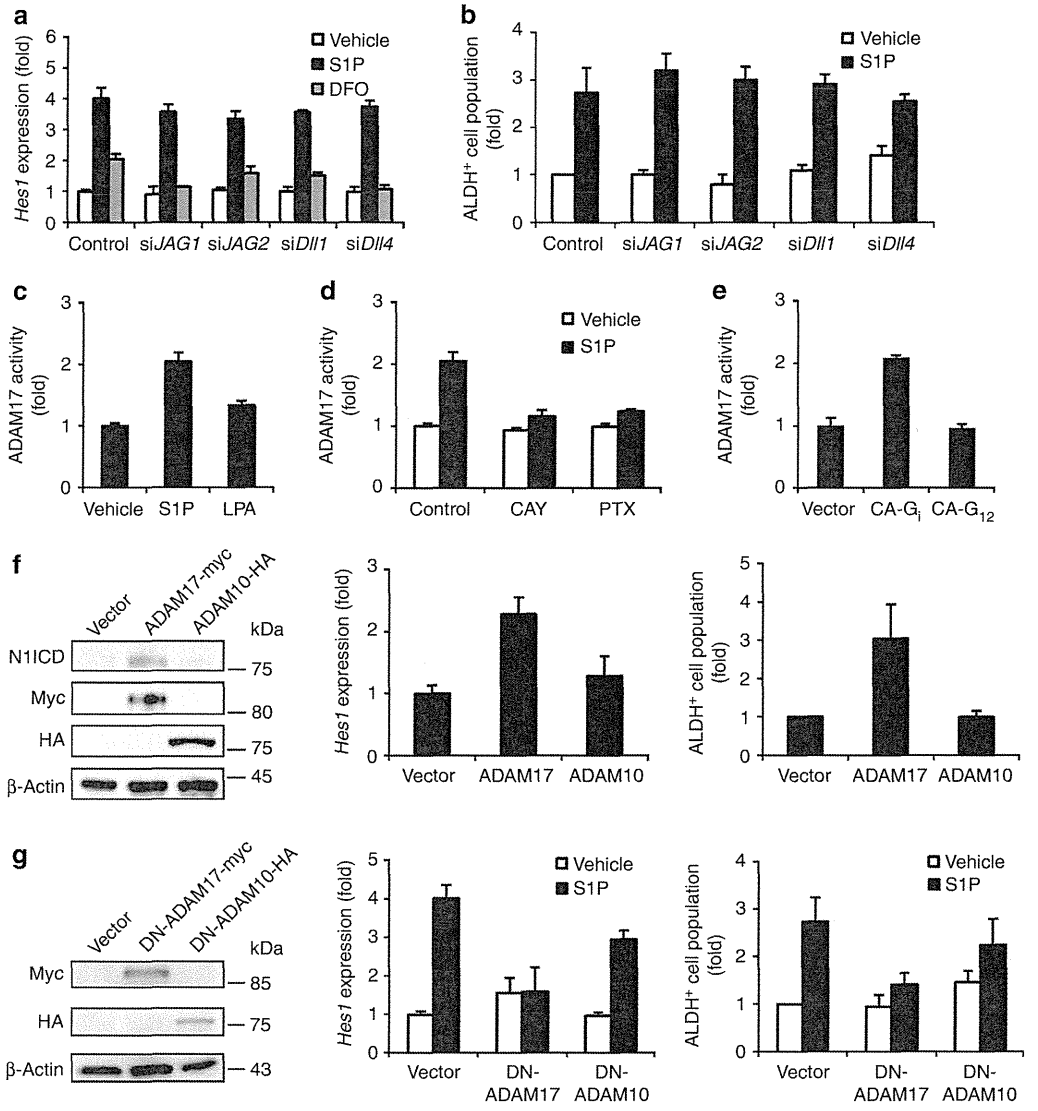

Figure 3 | S1P increases ALDH-positive cell population without Notch ligands. (**a**) Effects of siRNA against *Jagged1*, *Jagged2*, *Dll1* and *Dll4* on desferoxamine- or S1P-induced *Hes1* expression. Data represent mean ± s.d. ($n=3$). (**b**) Effects of siRNA against *Jagged1*, *Jagged2*, *Dll1* and *Dll4* on S1P-induced increase in ALDH-positive cell population. Data represent mean ± s.d. ($n=3$). (**c**) Stimulation with S1P (100 nM, 4 h) increased ADAM17 enzyme activity. Data represent mean ± s.d. ($n=3$). (**d**) S1P-induced ADAM17 activation was inhibited by CAY10444 (10 μM) and PTX (0.1 μg ml^{-1}). Data represent mean ± s.d. ($n=3$). (**e**) ADAM17 activation was induced by the overexpression of CA-G_i, but not by CA-G_{12}. Data represent mean ± s.d. ($n=3$). (**f**) Immunoblotting of N1ICD in ADAM17-myc- and ADAM10-HA-overexpressed MCF-7 cells. The expression of plasmids was confirmed using tag-specific antibody. Effects of overexpression of ADAM17 or ADAM10 on *Hes1* expression in MCF-7 cells. Effects of overexpression of ADAM17 or ADAM10 on ALDH-positive cell population in MCF-7 cells. Data represent mean ± s.d. ($n=3$). (**g**) Effects of DN mutants of ADAM17 or DN-ADAM10 on S1P-induced *Hes1* expression and the ALDH-positive cell population. Data represent mean ± s.d. ($n=3$). Expression levels were normalized to glyceraldehyde 3-phosphate dehydrogenase messenger RNAs.

the proportion of ALDH-positive cells in the tumour paralleled the *in vitro* results, suggesting a stem cell hierarchy (Fig. 6f). Histological analysis and double staining suggest that it is unlikely that the enhanced incidence of tumour formation by expression of SphK1 was due to cell differentiation. To examine whether S1PR3 and ALDH1 were co-expressed in the same cell, we performed double staining of ALDH1 and S1PR3 using xenografted tumour section (Supplementary Fig. 18). The number of ALDH1- and S1PR3 double-positive cells was increased in tumours derived from the SphK1-overexpressing ALDH-positive cells, compared with control and SphK2-overexpressing ALDH-positive cells. In addition, knockdown of *S1PR3* significantly inhibited the tumorigenicity of SphK1-overexpressing ALDH-positive cells, whereas knockdown of *S1PR2* had little effect (Fig. 6g). Furthermore, chronic administration of the S1PR3 antagonist TY52156 significantly inhibited the tumorigenicity of SphK1-overexpressing ALDH-positive cells (Fig. 6h). Taken together, both *in vitro* and *in vivo* results suggest that enhanced expression of SphK1 accelerated tumour formation of CSCs via S1PR3.

Patient-derived CSCs contain SphK1$^+$/ALDH1$^+$ cells. We further extended our observations to primary cell culture. To examine *S1PR3* expression level in breast CSCs, we performed qPCR using secondary mammospheres from patient-derived tumour[8] (Supplementary Table 1). Similar to MCF-7 cells, *S1PR3* was highly expressed in ALDH-positive cells derived from breast cancer patient (Fig. 7a). In addition, we evaluated whether there

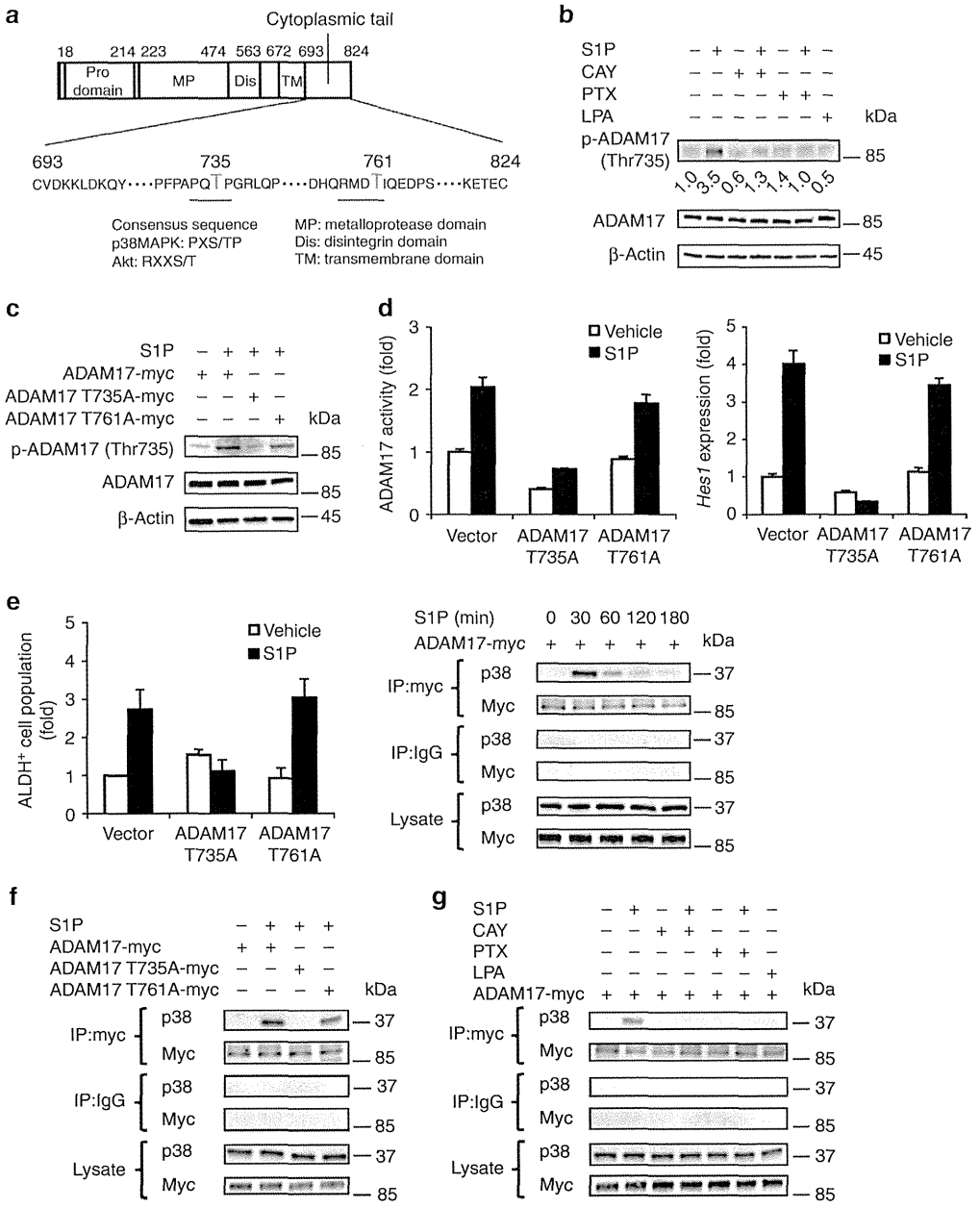

Figure 4 | S1P-induced ADAM17 activation via p38MAPK. (**a**) A schematic of the ADAM17 cytoplasmic domain mutants. (**b**) S1P-induced phosphorylation of ADAM17 at Thr735 was analysed by immunoblotting with a phospho-ADAM17 (Thr735)-specific antibody. (**c**) MCF-7 cells were transfected with ADAM17-T735A-myc or ADAM17-T761A-myc mutants and were then immunoblotted with phospho-ADAM17 (Thr735)-specific antibodies. (**d**) Effects of ADAM17-T735A and ADAM17-T761A mutants on S1P-induced ADAM17 activation, *Hes1* expression and ALDH-positive cell population. Expression levels were normalized to glyceraldehyde 3-phosphate dehydrogenase messenger RNAs. Data represent mean ± s.d. ($n=3$). (**e**) MCF-7 cells transfected with myc-tagged ADAM17 were either treated or untreated with S1P (100 nM) for the indicated times. The cells were then lysed and subjected immunoprecipitation with myc-specific antibodies, followed by p38MAPK-specific immunoblotting. (**f**) MCF-7 cells were transfected with myc-tagged ADAM17-T735A or T761A and stimulated with S1P (100 nM) for 30 min. The cells were then lysed and subjected to immunoprecipitation with myc-specific antibodies, followed by p38MAPK-specific immunoblotting. (**g**) MCF-7 cells transfected with myc-tagged ADAM17 were treated with S1P (100 nM) or LPA (100 nM) for 30 min in the presence or absence of CAY10444 (10 μM) or PTX (0.1 μg ml^{-1}). The cells were lysed and subjected to immunoprecipitation with myc-specific antibodies, followed by p38MAPK-specific immunoblotting.

were co-expressions of SphK1/ALDH1 or S1PR3/ALDH1 in breast CSCs by immunochemistry. Double staining demonstrated that these patient samples contained SphK1- and ALDH1 double-positive cells or S1PR3- and ALDH1 double-positive cells (Fig. 7b,c). We further evaluated whether SphK1, ADAM17 and N1ICD were co-expressed in the same cell. As a result, patient-derived tumour cells contained triple-positive cells (Fig. 7d). These data suggest that SphK1/S1PR3/Notch signalling is present in CSCs derived from breast cancer patient.

Discussion

In the present study, we used ALDH assays to identify regulators in CSCs, and determined that S1P/S1PR3 signalling and

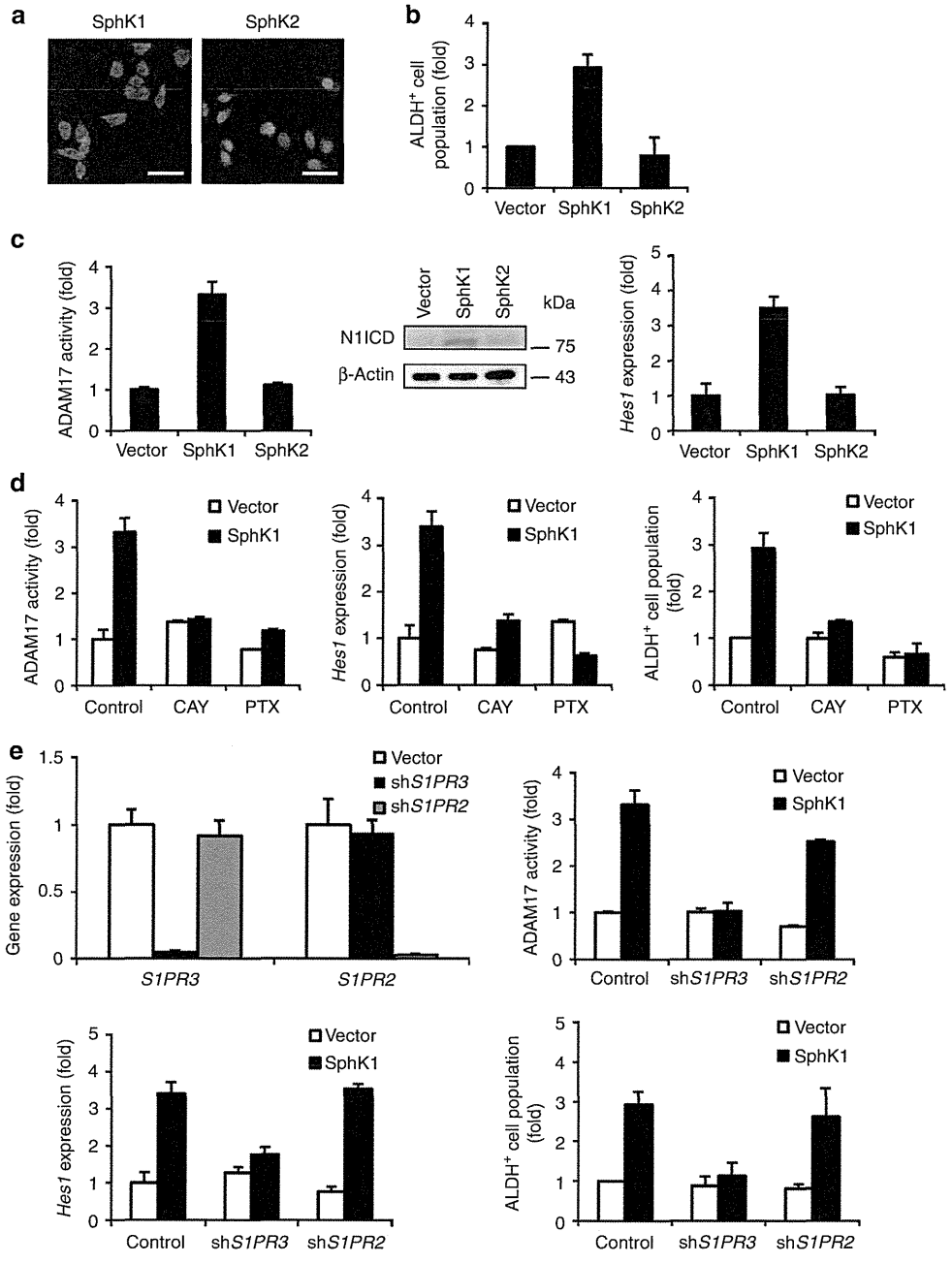

Figure 5 | Role of SphK1 in ALDH-positive cell population. (**a**) Expression of SphK in MCF-7 cells. Plasmid vectors encoding FLAG-tagged SphK1, or HA-tagged SphK2 were transfected into MCF-7 cells before SphK protein levels in cells were analysed by immunostaining. The scale bar indicates 20 μm. (**b**) Effects of SphK1 and SphK2 on the ALDH-positive cell population. Data represent mean ± s.d. ($n=3$). (**c**) Effects of SphK1 and SphK2 on ADAM17 activity, NICD production, and *Hes1* expression. Data represent mean ± s.d. ($n=3$). (**d**) Effects of CAY10444 (10 μM) and PTX (0.1 μg ml^{-1}) on the SphK1-induced ADAM17 activity, *Hes1* expression and ALDH-positive cell population. Data represent mean ± s.d. ($n=3$). (**e**) Expression level of S1P receptor in shRNA-transduced MCF-7 cells. Effects of shRNAs against *S1PR3* and *S1PR2* on the SphK1-induced ADAM17 activity, *Hes1* expression and ALDH-positive cell population. Data represent mean ± s.d. ($n=3$). Expression levels were normalized to glyceraldehyde 3-phosphate dehydrogenase messenger RNAs.

subsequent Notch activation resulted in an increase in the CSCs in several types of cancer (Fig. 8). S1PR3 antagonist inhibited the tumorigenicity of SphK1-overexpressed breast CSCs. Furthermore, breast cancer patient-derived CSCs contained SphK1$^+$/ALDH1$^+$ cells or S1PR3$^+$/ALDH1$^+$ cells. The findings presented here broaden our understanding of the role of lipids in CSC biology, and have significant clinical implications.

We found that S1P has the ability to induce proliferation of several types of CSCs, as stimulation with S1P activates Notch signalling, a key stem cell pathway. As such, S1P might have various roles in stem/progenitor cells. Indeed, S1P has been shown to maintain self-renewal of human embryonic stem cells in cooperation with platelet-derived growth factor[36]. Human-induced pluripotent stem cells have also been shown to express *S1PR3* messenger RNAs, although their biological effects in induced pluripotent stem cells are yet to be elucidated[37]. We postulate that S1P might have self-renewal properties, and play a key role in stem cell regulation.

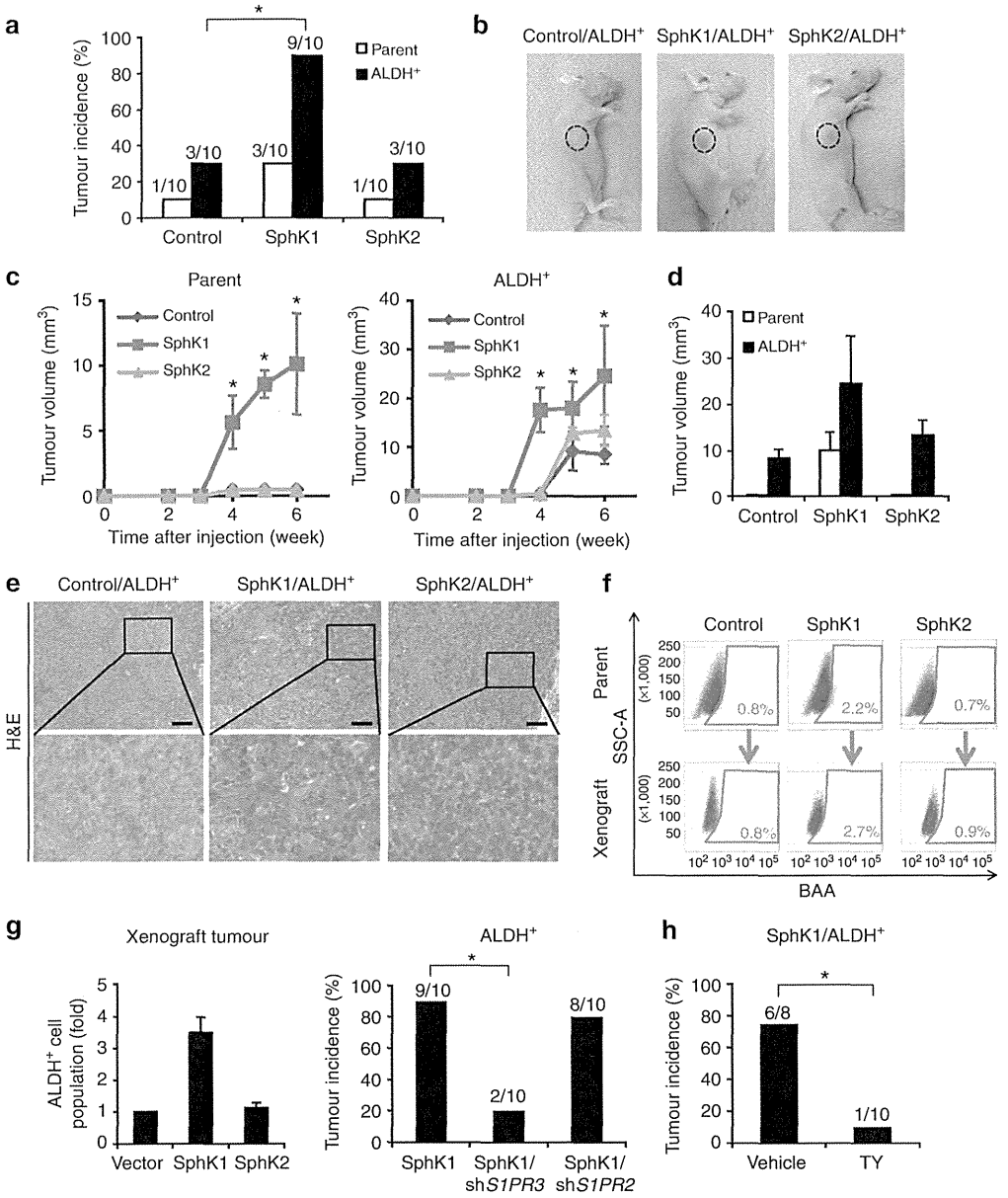

Figure 6 | SphK1 increases CSC-mediated tumour formation in a mouse xenograft model. (**a**) Balb/c nude mice were subcutaneously injected with 1×10^5 vector- or SphK-transfected MCF-7 cells. Tumour formation was indicated by tumours/injections at 6 weeks post injection. The *P* value was calculated using the Fisher's exact test. Bonferroni correction was applied for multiple comparisons. $^*P<0.05$ versus control. (**b**) Photographs of representative nude mice transplanted with ALDH-positive cells, SphK1-overexpressing ALDH-positive cells and SphK2-overexpressing ALDH-positive cells. (**c**) Tumour growth curves in the nude mice injected with parent or ALDH-positive cells. Tumour volume is presented as the mean ± s.d. ($n=10$). Kruskal–Wallis test, followed by the Steel–Dwass was used to determine significance. $^*P<0.05$ versus control. (**d**) Tumour volumes at 6 weeks post injection. Data represent mean ± s.d. ($n=10$). (**e**) Hematoxylin/eosin (H&E)-stained sections of tumour xenografts derived from vector-, SphK1-, and SphK2-overexpressing ALDH-positive cells. Scale bar, 100 μm. (**f**) Representative flow cytometry analysis of ALDH activity in the xenograft tumours derived from vector-, SphK1-, and SphK2-overexpressing ALDH-positive cells. The graph indicates ALDH-positive cell population in xenograft tumours. Data represent mean ± s.d. ($n=3$). ALDH-positive cells were able to regenerate the phenotypic heterogeneity in the xenograft tumours of nude mice. (**g**) Balb/c nude mice were subcutaneously injected with 1×10^5 vector-, *S1PR3*- or *S1PR2*-knockdown cells from SphK1-overexpressing ALDH-positive cells. Tumor formation was indicated by tumours/injections at 6 weeks post injection. The *P* value was calculated using the Fisher's exact test. Bonferroni correction was applied for multiple comparisons. $^*P<0.05$ versus control. (**h**) TY52156 or vehicle was inserted in subcutaneously implanted Alzet osmotic pumps before injection of 1×10^5 SphK1-overexpressing ALDH-positive cells. Tumour formation was indicated by tumours/injections at 6 weeks post injection. The *P* value was calculated using the Fisher's exact test. $^*P<0.05$ versus control.

We also identified S1P-induced Notch activation without Notch ligands. Consistent with our observations, previous studies have shown that ADAM17 mediates ligand-independent Notch activation, while ADAM10 is ligand dependent[38,39]. Another study has shown that soluble form of Jagged1 activates Notch signalling without cell–cell contact[40]. Furthermore, a recent study showed that multiple GPCRs, including the S1PR, resulted in shedding of TGFα via ADAM17 activation in HEK293 cells[41]. Within the S1PR family, S1PR3 has higher intrinsic activity for shedding. These data strongly support a signalling pathway